THE APPLICATION OF VLB INTERFEROMETRY TO EARTH MEASUREMENTS

Contract NSR 09-015-079

PHASES I, II, III, AND IV

FINAL REPORT

Principal Investigators

(Phase IV)

Dr. Dale F. Dickinson
Radio Astronomer
Smithsonian Astrophysical Observatory

Dr. Mario D. Grossi
Radio Physicist and Engineer
Smithsonian Astrophysical Observatory

April 1973

Written by
Richard D. Michelini

Prepared for

National Aeronautics and Space Administration
Washington, D.C. 20546

Smithsonian Institution
Astrophysical Observatory
Cambridge, Massachusetts 02138

THE APPLICATION OF VLB INTERFEROMETRY TO EARTH MEASUREMENTS

Contract NSR 09-015-079

PHASES I, II, III, AND IV

FINAL REPORT

Principal Investigators

(Phase IV)

Dr. Dale F. Dickinson
Radio Astronomer
Smithsonian Astrophysical Observatory

Dr. Mario D. Grossi
Radio Physicist and Engineer
Smithsonian Astrophysical Observatory

April 1973

Written by
Richard D. Michelini

Prepared for

National Aeronautics and Space Administration
Washington, D.C. 20546

Smithsonian Institution
Astrophysical Observatory
Cambridge, Massachusetts 02138

302-116

TABLE OF CONTENTS

THE APPLICATION OF
VLB INTERFEROMETRY TO EARTH MEASUREMENTS

Final Report

Contract NSR 09-015-079

1. INTRODUCTION

1.1 Foreword

This report summarizes the results of a four-phase development of capability in very long-baseline interferometry (VLBI) at the Smithsonian Astrophysical Observatory (SAO).

The results reported herein are principally those of Phase IV. This phase initiated the series of field experiments made under the contract and produced significant results in utilizing both natural objects and artificial satellites as fringe-producing sources. The investigatory phases (I and II) and the hardware phase (III), in which most of the equipment was designed and fabricated, have been reported in individual documents [1–4]. Where necessary for a complete description of the results of Phase IV, work done in the preceding phases has been included in this report.

1.2 Program Objectives

The objectives of the VLBI program at SAO are to:

1. Develop the capability to collect, process, and analyze VLBI data.

2. Determine experimentally the accuracy now attainable with VLBI and, within the constraints imposed by this accuracy, initiate a program of VLBI observations for geophysical applications.

3. Identify all significant error sources and devise means for eliminating or correcting these errors.

4. Develop a long-range plan for applying VLBI techniques to a program of earth-physics measurements.

1.3 Description of the Phases

Phase I

SAO Project Number:	17120-317
Project Title:	The Investigation of Continental Drift
Funding Agency:	NASA (OSSA)
Contract Number:	NSR 09-015-079
Period of Performance:	1 April to 30 September 1968
Coinvestigators:	Mr. Carlton G. Lehr, Dr. Ursula B. Marvin, and Dr. Paul A. Mohr

Phase I was an analysis of techniques that could be used in the study of continental drift. The results, presented in the Phase I Final Report, showed that very long-baseline interferometry was potentially a powerful technique for this purpose.

Phase II

SAO Project Number:	17120-317
Project Title:	The Investigation of Continental Drift
Funding Agency:	NASA (OSSA)
Contract Number:	NSR 09-015-079
Period of Performance:	1 October 1968 to 15 March 1969
Principal Investigator:	Dr. Mario D. Grossi

During Phase II, an experimental program was formulated to investigate VLBI techniques further.

Phase III

SAO Project Number:	17170-317
Project Title:	The Application of VLB Interferometry to Earth Measurements
Funding Agency:	NASA (OSSA)
Contract Number:	NSR 09-015-079
Period of Performance:	15 March to 30 October 1969
Principal Investigators:	Dr. Mario D. Grossi and Dr. Dale F. Dickinson

During Phase III, the design, procurement, and construction of the equipment for the experimental program developed in Phase II were completed. To facilitate the gathering of data, two identical recording VLBI terminals were constructed. One is normally used at the Agassiz 84-ft radio telescope, and the second at another radio telescope. Data taken at each are processed on a special playback terminal at SAO and combined to determine the parameters of the baseline vector extending between the telescopes. The parameters obtained in this manner are to be compared with the results of an independent survey of the baseline between the telescopes.

Phase IV

SAO Project Number:	17170-317
Project Title:	The Application of VLB Interferometry to Earth Measurements
Funding Agency:	NASA (OSSA)
Contract Number:	NSR 09-015-079
Period of Performance:	1 November 1969 to 30 June 1970
Principal Investigators:	Dr. Mario D. Grossi and Dr. Dale F. Dickinson

1.4 Phase IV Effort

The primary goal of the Phase IV effort was to conduct initial validation tests to study the accuracy and sensitivity of several specific VLBI configurations. In particular, efforts were directed to

1. Attempt a series of interferometer measurements over baselines that had been independently surveyed and compare the data obtained by both techniques.

2. Attempt to obtain fringes from a radio source carried aboard a satellite already in orbit.

3. Attempt a series of measurements over a baseline on which one antenna can be moved by calibrated amounts or where two or more antennas exist close together at one of the terminals. The purpose of these measurements was to determine how accurately a differential change in baseline is reflected in the measured fringe information.

In accordance with the goals stated above, we undertook three sets of full-scale field experiments during Phase IV. Information for these experiments is given in Table 1. Experiment periods I and II yielded no natural-source fringes. Following a careful and thorough study of the data gathered during the experiments, a discussion of possible reasons for this failure is contained in Section 5.

We were successful in obtaining artificial-source fringes from data taken from ATS 5 transmissions during Experiment period II. Procedures and results are discussed in some detail in Section 5. From the correlation records corresponding to the fringes, we were able to observe and confirm the various PM-PSK frequencies impressed on the carrier signal between transmitting stations. However, it was not possible to attempt a determination of satellite position from the fringe data; only two stations were used, and at least three are required for an unambiguous result if ranging data are not available.

Table 1. VLBI experiment summary.

Experiment period	Session	Station coordinates	Frequency (MHz)	Baseline length (km)	Baseline length Wavelength (λ)	Observation period
I	1, 2, 3	Agassiz Station $\phi = 42°30'21\!.''71$ $\lambda = 288°26'45\!.''92$ H = 213.09 m	4850	4219.2*	68,051,600	25 November to 30 December 1969
		Owens Valley* $\phi = 37°13'53\!.''49$ $\lambda = 241°43'5\!.''64$ H = 1226.65 m				
II	4	Agassiz Station	1665 (natural sources)	4219.2*	23,426,900	27 February to 24 March 1970
		Owens Valley*	1550 (satellite source)	4219.2	21,741,700	
III	5, 6, 7	Agassiz Station	1665	14.46	80,289	15 July to 2 August 1970
		Haystack $\phi = 42°37'23\!.''44$ $\lambda = 71°29'18\!.''39$ H = 167.14 m				

*Baseline determination was also attempted with the Owens antenna moved 41.596 m due west.

When natural-source fringes were not forthcoming from the data taken between Agassiz and Owens Valley Radio Observatory (OVRO), a new set of experiment sessions, numbered 5 through 7, was undertaken between Agassiz and Haystack. These were conducted with station clocks directly compared before each observing session, thereby establishing more controlled timing conditions than were possible over transcontinental distances. The principal objectives of these short-baseline experiments were to assure ourselves that 1) the SAO 1-bit recording back ends were functioning properly in the field, 2) the timing equipment was adequately controlling station synchronization, and 3) performance of the front ends and frequency standards could be guaranteed by appropriate field tests. The Agassiz–Haystack sessions produced uniformly good results, and we were able to obtain up to nine sets of fringes from each of five different natural sources (Section 5).

On the basis of the progress made during Phase IV, we believe that all SAO-built equipment is functioning properly and that timing, phase, and frequency control can be ensured under field conditions. We are convinced that, in the future, fringes over transcontinental distances can be obtained by using the equipment and techniques developed under this program and that they will result in baseline parameter measurements of the predicted accuracy.

2. DESCRIPTION OF THE EXPERIMENTS

A number of VLBI experiments were conducted during the period of this report. These included the following:

1. C-band experiments between the Agassiz 84-ft radio telescope and the Owens Valley 130-ft radio telescope, utilizing natural radio sources.

2. L-band experiments between the same two sites, utilizing natural radio sources.

3. An experiment using signals from the ATS 5 satellite at 1550 MHz with the same two telescopes.

4. L-band experiments between the Agassiz and the Haystack telescopes over a baseline of 14.46 km.

Table 1 summarizes the details of these major field experiments.

In addition, the two back ends were tested in simulated experiments in which a signal from an artificial noise source was split into two parts, fed through the two back ends, and recorded on the two recorders. The two tapes were later correlated.

2.1 Observations

Natural sources observed included the following:

Source	Identification	Flux (1665 MHz)(f. u.)
3C84	Seyfert Galaxy	11
3C120	Seyfert Galaxy	4
3C147	Quasar	20
3C273	Quasar	29
3C279	Quasar	11
3C286	Quasar	13.5
3C309.1	Quasar	7.5
3C345	Quasar	6.5

Source	Identification	Flux (1665 MHz)(f. u.)
3C380	Quasar	13
3C454.3	Quasar	12
CTA 21	...	7
CTA 102	Quasar	10.2
P 1127-14	Quasar	6.2
P 2134+00	Quasar	11.3 (5010 MHz)
OH in W3	Spectral Line	

Several observations were made on each source during the time of common visibility at the two sites. The observations were repeated with the 130-ft antenna at Owens Valley moved to the extreme end of the track and then back to the zero position. The first and third experiments were conducted by using right circular polarization; the second, linear polarization.

The ATS 5 satellite observations were made during an extended test period when the ATS Project Office and its contractor, Applied Information Industries, Inc., in Moorestown, New Jersey, were conducting transmission and navigation measurements on transponded L-band signals from the spacecraft. As it happened, suppressed-carrier phase-shift-keyed (PSK) modulation, alternating between 83.3-kHz, 8.33-kHz, and 833-Hz modulation rates and extending for durations of 1 to 8 min each, were received by the interferometer; also recorded were periods of 5 to 10 sec of wide-band noise. Sporadic transmissions, possibly speech or data PSK-PSK modulation, were also received.

The ATS 5 satellite moves in a synchronous orbit, inclined to the equator by some 2°.5. Its ground track resembles a narrow, elongated ellipse, about 0°.5 longitude in width, whose center lies on the equator at about 105°W, the longitude of Denver. Its elevation at Agassiz is about 30° above the horizon, while at Owens Valley it is about 45°. Pointing information was supplied by the ATS Project Office at NASA/GSFC. Because of the relatively stationary position of the spacecraft, tracking it presented no problem, and observations could be conducted with the antennas under manual control.

2.2 Simulation Tests

Simulation tests with the two back ends in the same place were performed with various levels of input signal. A variable attenuation pad was used, and the signal with the attenuator set at 3 db was approximately the same strength as the signal recorded from the quasar 3C273. The correlation of the data on the two tapes showed that integration over 10 records or even fewer (corresponding to an integration time of about 2 sec) was quite adequate to produce a correlation peak for signals recorded at 0-db level. For signals recorded at a setting as low as 9 db, a good correlation peak was obtained with an integration time of about 20 sec.

3. INSTRUMENTATION

We chose to develop a hybrid VLBI recording and playback system rather than adopt either the well-proved Mk I system of the National Radio Astronomy Observatory (NRAO) or a relatively straightforward analog correlator. This choice was made to gain greater recording durations, extended bandwidth potential, and maximum utilization of available data-handling equipment, and at the same time retain compatibility with the Mk I system.

A flexible VLBI instrumentation system was developed for routine observations. The system records digital data on videotape in the field and later generates conventional digital magnetic tapes for programed correlation in a high-speed, general-purpose computer. By selection of an appropriate data rate, these tapes can be made compatible with the present NRAO Mk I format. In addition, the major components were chosen so that they might later be incorporated into the Mk II system, which was then under development at NRAO and which became operational in early 1971. The Mk II is a high-density, wide-bandwidth system that uses direct videotape correlation. Other, more immediate advantages of videotape recorders are low initial cost, low cost per bit, long recording time, portability, and minimal requirements for installation in the field. This section describes the instrumentation back end, including the video converter, recording system, and computer-compatible reformating units. Station timekeeping, which is integral with the recording format, is also discussed.

3.1 System Description

The instrumentation developed by SAO to make VLBI observations for geophysical measurements was based on the conventional 1-bit quantization and correlation techniques of Weinreb [5]. Consequently, this approach has the advantage of compatibility with the large digital computers available for correlation analysis and fringe processing. In its present

configuration, the system permits the immediate use of available computer tape drives, programs, and computer systems. It also recognizes the acceptance among observers of standard data-recording and processing formats. Each component was designed or selected to permit compatibility with both Mk I and Mk II VLBI formats as incorporated into systems designed by NRAO. Furthermore, with use of the basic video recorder, the system can be expanded to permit much higher data rates (video bandwidths). The overall system specifications are listed in Table 2. The recording system used at OVRO is shown in Figure 1a. This arrangement was typical at all stations.

The idea of commonality or compatibility with existing VLBI data systems was an important factor in the design of the SAO system. Because of their worldwide nature, many VLBI experiments are cooperative ventures; consequently, it is important that the equipment be built with a standard format in mind. Among most United States investigators, this format is the one originated by NRAO and incorporated into a number of systems constructed by NRAO, Massachusetts Institute of Technology (MIT), and Cornell/Arecibo. To date, this compatibility has been exploited in a baseline with the SAO system at one terminal and a Mk I-type back end constructed by MIT at the other. The basic features of this format are a sampling rate of 720 kbit/sec and a digital output on 7-track, IBM-compatible magnetic tape.

While this standard format would provide adequate bandwidth for initial geodetic VLBI studies, it was desirable to expand the data capacity to equal the maximum capacity of the peripheral computer equipment available to SAO. Consequently, with minor format changes, the capability of operating at a sampling rate of 960 kbit/sec was added to the system.

The principal recording and playback innovations follow from the use of a TV-type, rotary-head, helical-scan magnetic-tape recorder as the primary digital-data recorder. Quantization and sampling procedures are similar to those developed by Bare [6, 7] for IBM-compatible digital recorders, but the record and playback techniques have been designed to accommodate wide-bandwidth, self-clocked digital data in a standard TV-frame format. The present system operates at sampling rates of 714, 720, and 960 kbits/sec

Table 2. System specifications.

Channel bandwidth:	Selectable — 350 kHz, 480 kHz, 1 MHz, 2 MHz (-20 db bandwidths) Limited to 480 kHz by available digital recorders.
Frequency stability:	2.5×10^{-12} 100-sec averaging with rubidium standard 1.5×10^{-13} 100-sec averaging with hydrogen maser
Integration time:	Up to 5 hours, depending on frequency standards used.
Time (epoch) synchronization:	±5 μsec on initial setting
Epoch traceability:	±2 μsec to UTC (USNO)
Time-record resolution:	±1 μsec
Correlation time-delay resolution:	100 to 200 nsec, depending on signal-to-noise ratio

Figure 1a. The VLBI recording system shown installed at OVRO.

using direct bipolar recording and reformats the data on 9-track digital tape for entry into a CDC 6400 computer. The several bandwidths and formats used by SAO during the program are given in Table 3. Data rates up to 5 Mbits/sec can be accommodated if special encoding and processing are used in recording. The playback terminal, which was maintained at SAO, is shown in Figure 1b.

A detailed description of the recording and playback system is given by Michelini [8].

3.2 Instrumentation Variations

At each of the three observing sessions held during the program, the instrumentation differed in several details. In general, the differences concerned only the antenna and the front end (RF systems), which varied according to the baselines and the sources (natural or artificial) used. To a lesser extent, the timing and frequency-control methods were modified for each session. No changes, however, were made in the video recording and playback system described in Section 3.1, with the exception of small modifications in the bit rate (e.g., 714 and 720 kbits/sec).

The primary observing periods were the following:

Period	Session	Baseline Stations	Dates of Observations
I	1, 2, 3	Agassiz–OVRO	25 November–13 December 1969
II	4	Agassiz–OVRO	27 February–24 March 1970
III	5, 6, 7	Agassiz–Haystack	15 July–2 August 1970

A summary of the major instrumentation specifications at each station is given in Table 4.

The Agassiz radio telescope consists of an 84-ft parabolic antenna with a Cassegrain dual-mode feed system connected to an L- or C-band parametric amplifier. A block diagram of the complete VLBI front end is given in Figure 2a. The total power output of the paramp is heterodyned in a crystal

Table 3. Various bandwidths* and recording formats of the VLBI back end.

	(a)	(b)	(c)	(d)	(e)
Bandwidth (kHz)	350	350	350	350	480
Clock frequency to formater (MHz)	5.04 (Mk I format)	5	5.04	5	6.72
Sampling rate (bits/sec)	720K	714,285.715	720K	714,285.715	960K
Bit period (μsec)	1.3888	1.4	1.3888	1.4	1.0417
Video frame period (msec)	16-2/3	16.80000	16-2/3	16.80000	16.7676
rate (per sec)	60	59.52381	60	59.52381	59.64096
Bits/video frame	12,000	12,000	12,000	12,000	16,096
Digital record length					
in bits	139,752	139,752	151,800	151,800	202,400
msec	194.1000	195.6528	210.8333	212.5200	210.8401
video frames	11.646	11.646	12.650	12.650	12.575
IR gap length					
in bits	4248	4248	4200	4200	6848
msec	5.900	5.9472	5.8333	5.8800	7.1387
video frames	0.354	0.354	0.350	0.350	0.425
Total digital record length					
in bits	144,000	144,000	156,000	156,000	209,248
msec	200.000	201.6	216.6667	218.400	217.9788
video frames	12.000	12.000	13.000	13.000	13.000

*Bandwidths are currently limited by the recording rate of the digital recorders used.

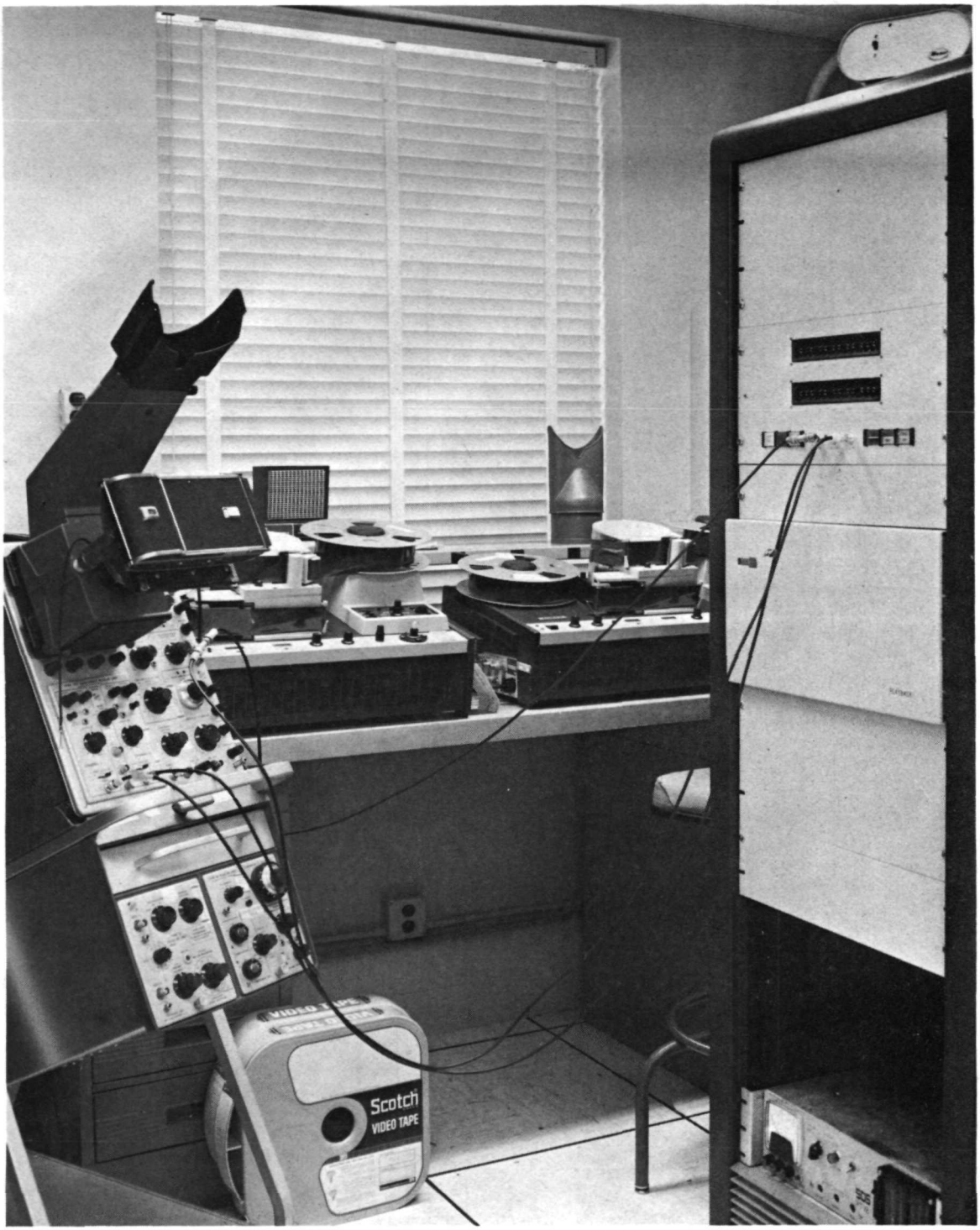

Figure 1b. The VLBI playback system.

Table 4. Summary of major instrumentation specifications.

Observing session	Station	Dish diameter (ft)	Focal system	Antenna temperature (K)	System temperature (K)	Observing frequency (MHz)	Polarization	Receiver type	Sideband selection	Local-oscillator system	Number of IF conversion stages	Intermediate frequency to video converter (MHz)	Sampling rate (kbits/sec)	Frequency standard	Station synchronization
1, 2, 3	Agassiz	84	Cassegrain	30	180	4850	Right circular	Uncooled single-stage paramp	Lower sideband	Phase-locked multiplier	4	150	720	H maser (SAO)	Loran C
	OVRO	130	Prime focus	42	190	4850	Right circular	Uncooled single-stage paramp	Lower sideband	Phase-locked multiplier	3	30	720	Rb cell HP 5065A	Loran C and portable clock
4	Agassiz	84	Cassegrain	35	200	1665 and 1550	Linear	Uncooled single-stage paramp; transistor amplifier*	Lower sideband	Phase-locked multiplier	4	150	714	Rb cell HP 5065A	Loran C
	OVRO	130	Prime focus	45	225	1665 and 1550	Linear	Uncooled single-stage paramp; transistor amplifier*	Lower sideband	Phase-locked multiplier and synthesizer doubler	3	30	714	Rb cell HP 5065A	Loran C and portable clock
5, 6, 7	Agassiz	84	Cassegrain	35	200	1665	Right circular	Uncooled single-stage paramp	Lower sideband	Phase-locked multiplier	4	150	714	H maser and Rb cell†	Portable clock
	Haystack	120	Cassegrain	26	310	1665	Right circular	Uncooled single-stage paramp	Lower sideband	Phase-locked multiplier	4	30	714	Rb cell‡ and H maser**	Portable clock

*For ATS 5 observations.

†Used on some runs of session 6.

‡Sessions 5 and 6.

**Maser used as first and second local oscillator reference only.

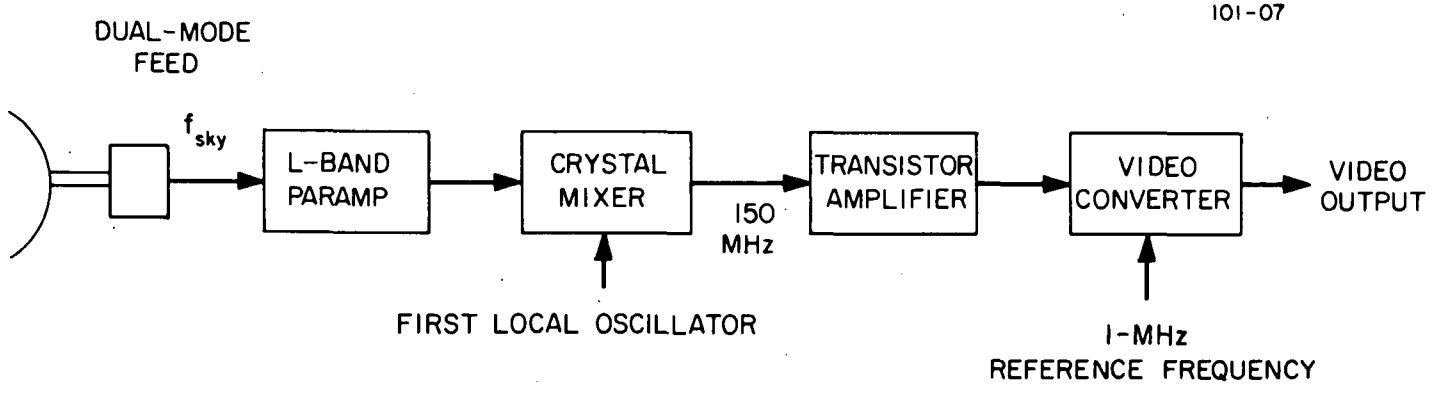

Figure 2a. Basic VLBI front-end system used at Agassiz.

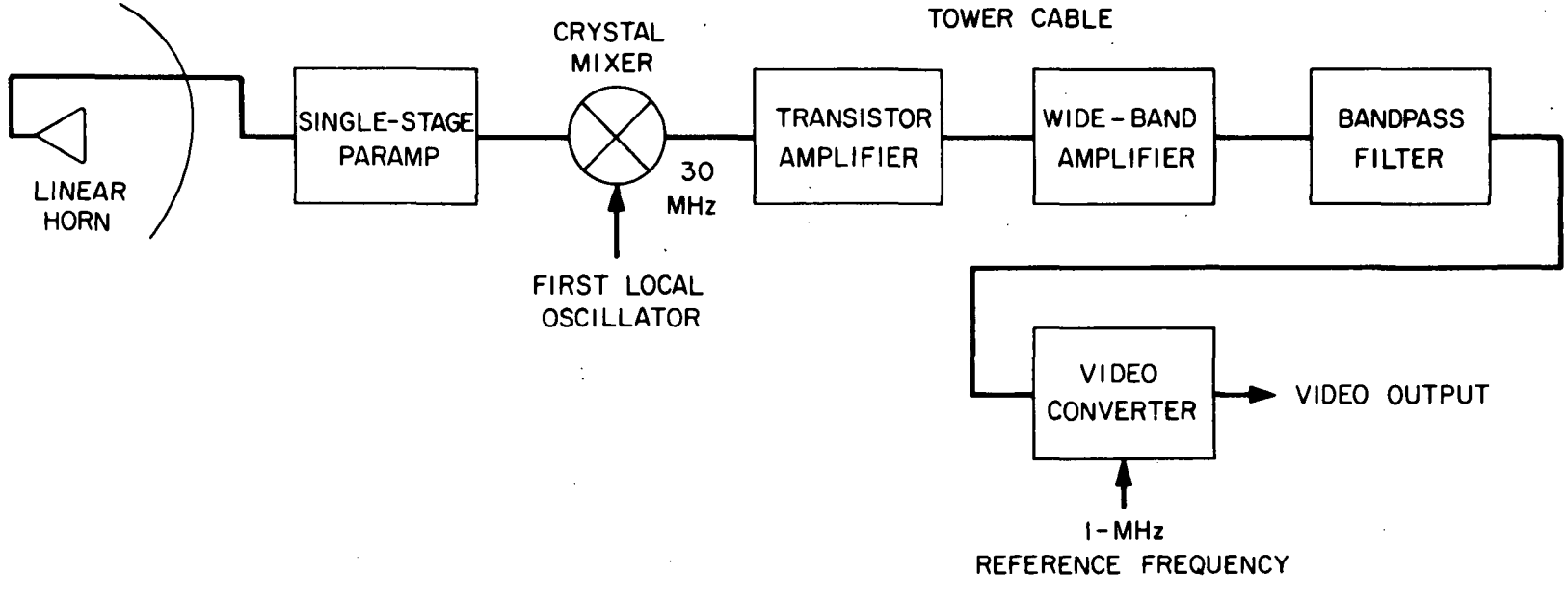

Figure 2b. Basic VLBI front-end system used at OVRO.

mixer with the output of the first local oscillator (which is phase-locked to the frequency standard). The resulting 150-MHz signal is then fed to a transistor amplifier whose output goes to the video converter.

The radio telescope at Owens Valley is a 130-ft parabolic antenna with a prime-focus feed system. Figure 2b shows the basic front-end configuration. Both C- and L-band paramps were used in different observation sessions, both receivers being single-stage uncooled units. For 6-cm operation, the first local oscillator was klystron-generated and phase-locked to a Rb-cell frequency standard (Figure 3) via a ×5 multiplier and a 1-MHz reference signal. At 18 cm, the phase-locked Rohde and Schwarz synthesizer output was frequency doubled and used directly as the local-oscillator input (Figure 4). The same HP 5065A Rb-cell frequency standard that was used at 6 cm was used for the 18-cm observations.

The 30-MHz IF signal was fed to a low-noise transistor amplifier, a wideband amplifier, and a bandpass IF filter and then converted to video in the video converter.

The Haystack radio telescope is a 120-ft parabolic antenna equipped with a Cassegrain feed system. For the observations described in this report, an L-band feed (R-box) and a parametric amplifier were used, followed by a tunnel diode amplifier. The phase-locked L-band local-oscillator frequency was derived from either a Rb-cell standard (first two sessions) or a hydrogen maser (last session). The IF from the first mixer was further converted to 30 MHz to be suitable for the video converter. A 5-MHz bandpass filter was used for image rejection at the input to the video converter. The Haystack front end is shown in Figure 5 as it was adapted for the SAO observations.

For the observations of the ATS 5 satellite, the strong L-band downlink signal level required that the paramp stages at both receiving terminals be disabled and that the transistor amplifiers normally employed as postamplifiers be used alone. Three receiving frequencies (1550.296, 1550.238, and 1550.000 MHz) were used, but the majority of modulated data were taken at

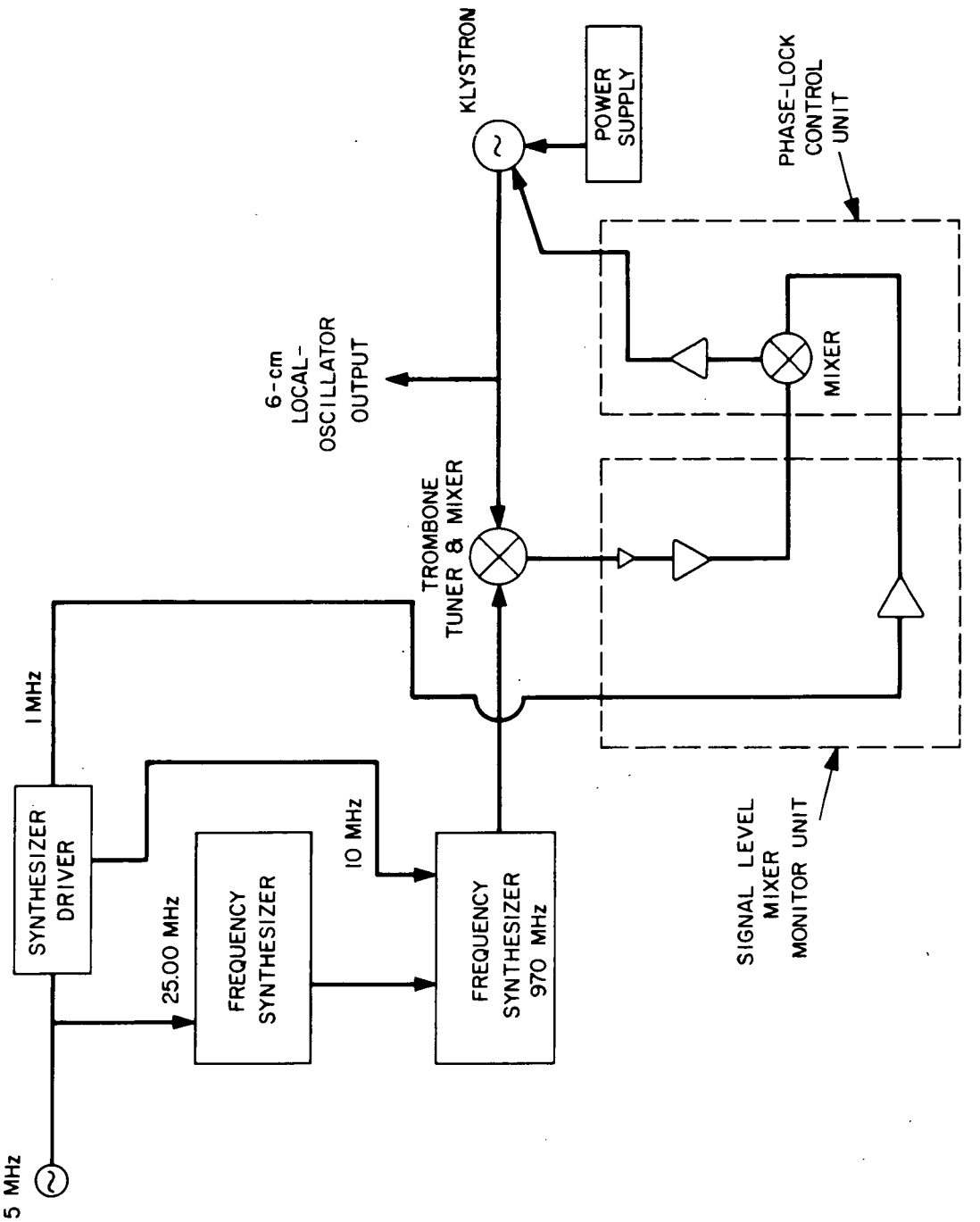

Figure 3. 6-cm local-oscillator system used at OVRO.

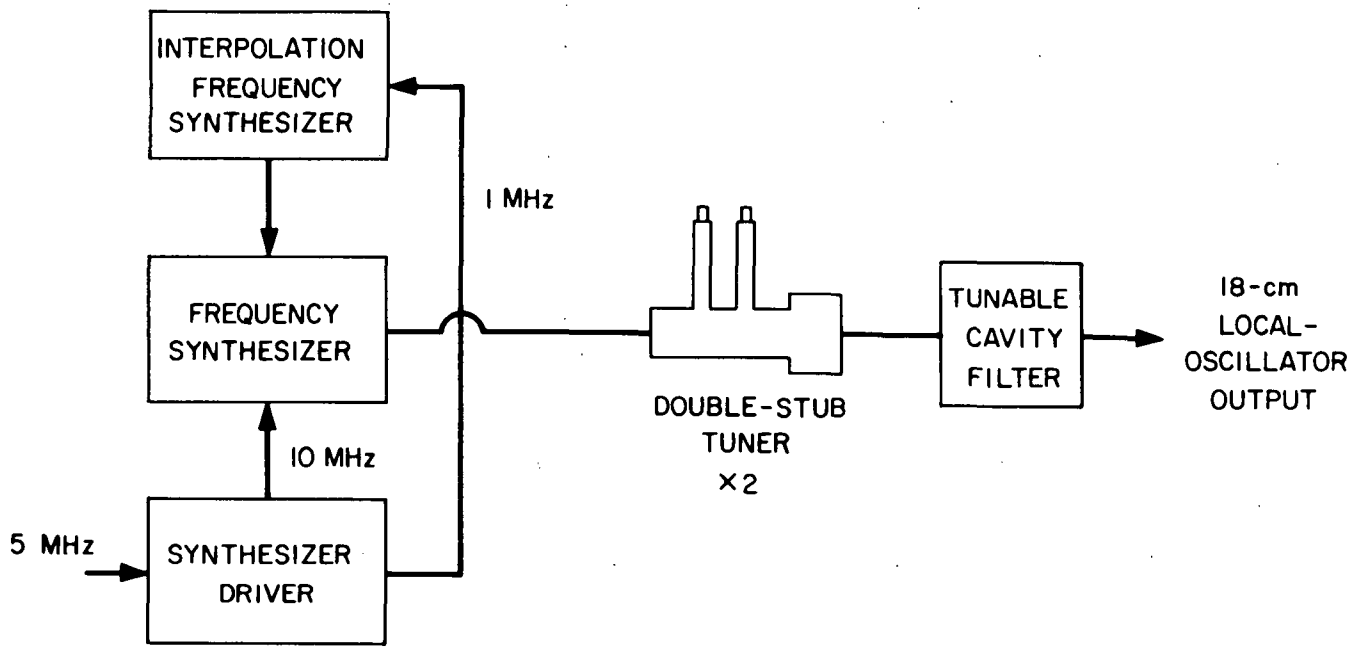

Figure 4. 18-cm local-oscillator system used at OVRO.

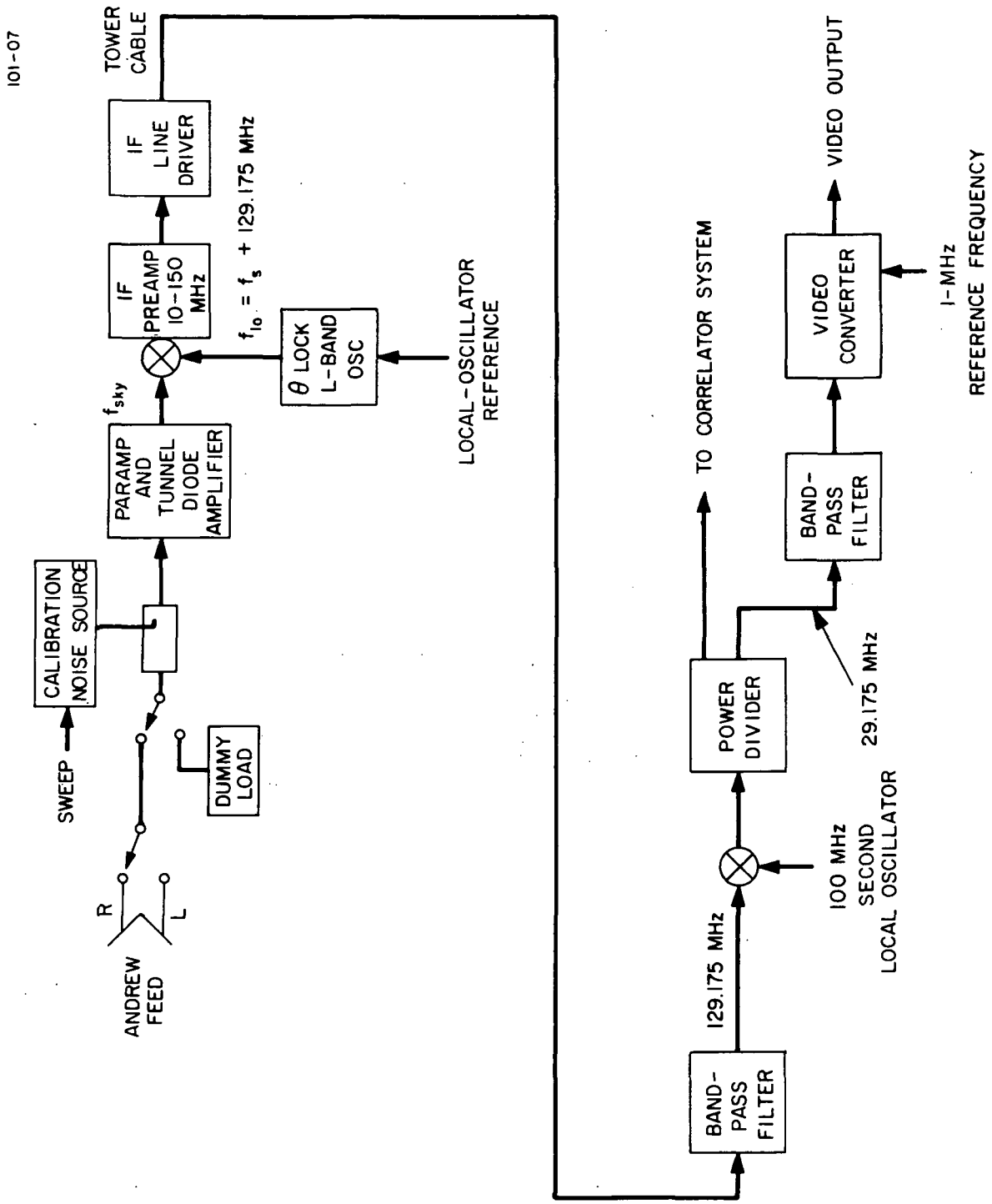

Figure 5. Basic VLBI front-end system used at Haystack.

1550.00 MHz, which was the normal wide-band L-band-to-L-band frequency translation mode. Except for the required retuning and some attenuation of the video level, procedures were identical to those used for observing natural (quasi-stellar) objects. Tracking of the source was accomplished manually, with slight corrections being applied to the calculated positions so that the detector output of the radiometer remained relatively constant. Pointing corrections to position the source in the beam were required about every half hour.

3.3 Significant Test and Setting-Up Procedures

To ensure that the instrumentation used in each VLBI observing session was operating properly and to determine sufficiently the time synchronization between sites, several system tests were made before and during actual field operation.

3.3.1 Phase stability

The most important test is that for phase stability of the local frequency standards and for the stability of the associated receiver RF link from feed to the video converter. Excursions in phase at the reference frequency are multiplied at RF and can cause significant loss of coherence in the correlated output.

Two phase tests were made on the installation at the Agassiz dish. The first measured phase jitter arising in the feed and RF/IF systems, excluding the frequency-control/local-oscillator system; the second test detected any signal-phase variations originating in the feed, RF/IF system, and frequency-control/local-oscillator chain.

In the first test arrangement, the phase output of the video converter was compared to a reference signal that was phase-locked to the test signal and the local-oscillator signal (Figure 6).

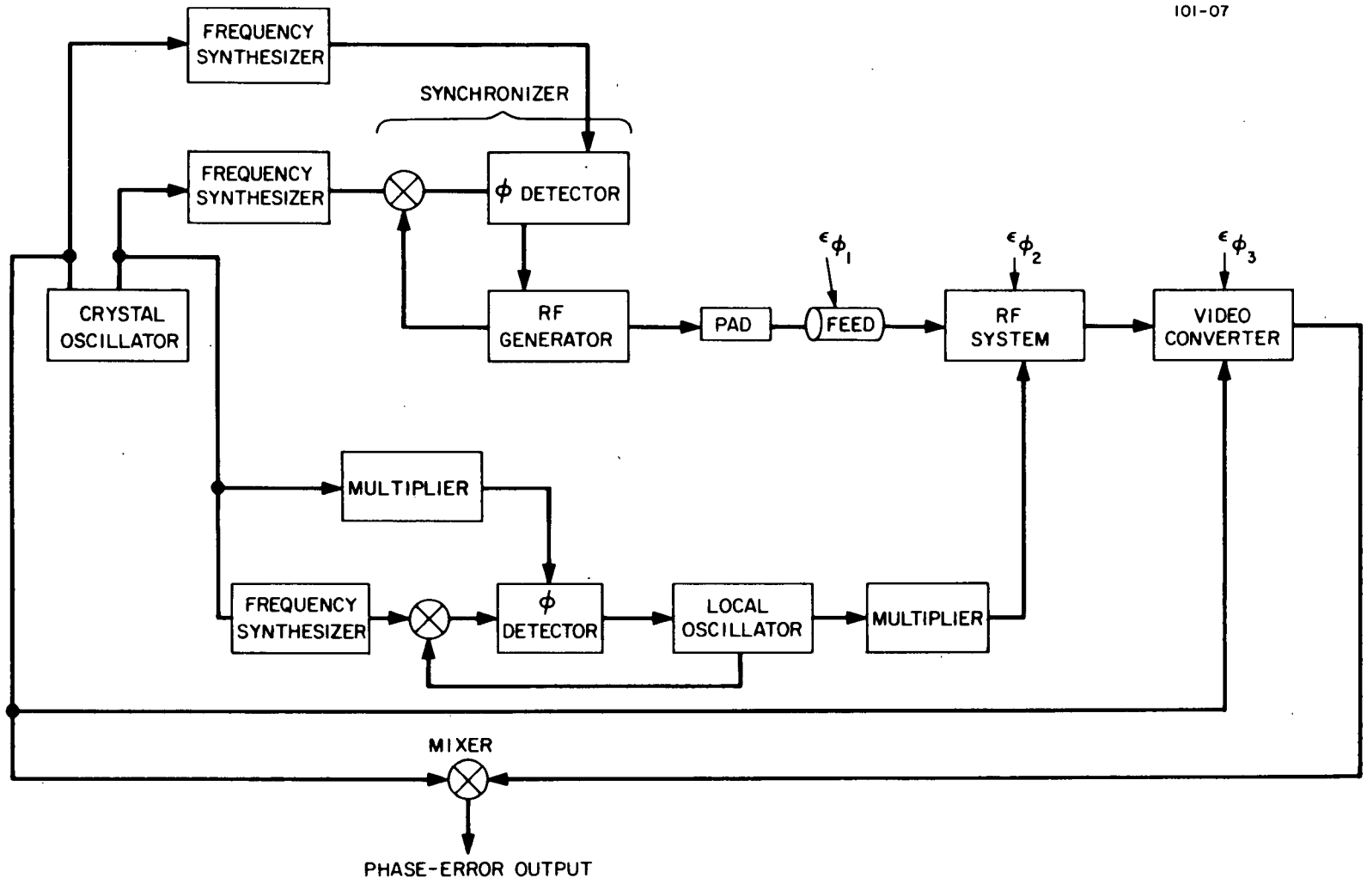

Figure 6. Arrangement for phase-stability test. Local-oscillator effects were not measured.

In the second test (Figure 7), the video-converter output was phase-compared with a reference that was phase-locked to the RF test signal injected into the feed. In this case, the local-oscillator signals in the receiver and video converter were phase-locked to an independent standard of high precision. A hydrogen-maser frequency standard, shown in Figure 8, was used in this test.

Tests made at Agassiz under these conditions confirmed that negligible phase drift or jitter was contributed by the maser frequency standard. However, spurious phase excursions, shown in Figure 9, were observed, amounting to between 30° and 40° in phase. In addition, low-frequency (60 and 120 cps) phase jitter was superimposed on the video output. In an effort to remove this instability, the following improvements were made:

1. Four new coaxial lines were laid to the Cassegrain focus to reduce 60-cps pickup caused by the drive-motor power leads.

2. A faulty RF connector was replaced.

3. The low-frequency response of the local-oscillator phase-lock loop was reduced by replacing the filter capacitors with smaller units.

4. The 1-MHz local-oscillator input to the video converter was isolated (via a digital synthesizer) from the 1-MHz maser signal used by the system clock.

After these changes were made, tests showed that no phase discontinuities remained and there was a marked reduction in 60- and 120-cps jitter, amounting to a maximum instantaneous excursion of ±3°. Figure 10 illustrates the final phase performance achieved.

The test described above was performed before the third observing session (Agassiz–Haystack). While the magnitude of the phase instabilities found was probably not large enough to account for the failure to obtain natural-source fringes during the two previous observing sessions, it is

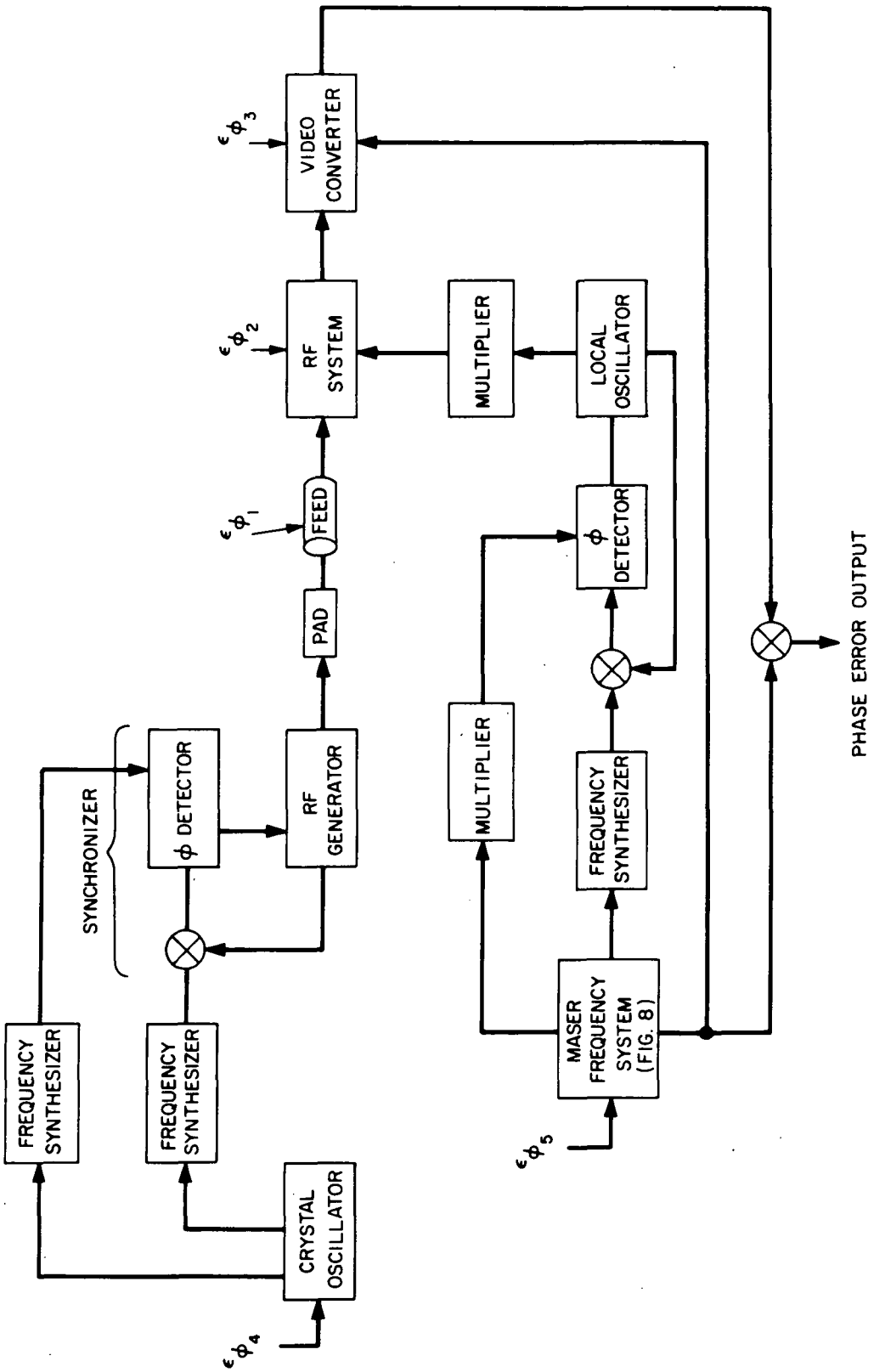

Figure 7. Arrangement for phase-stability tests, including local-oscillator effects.

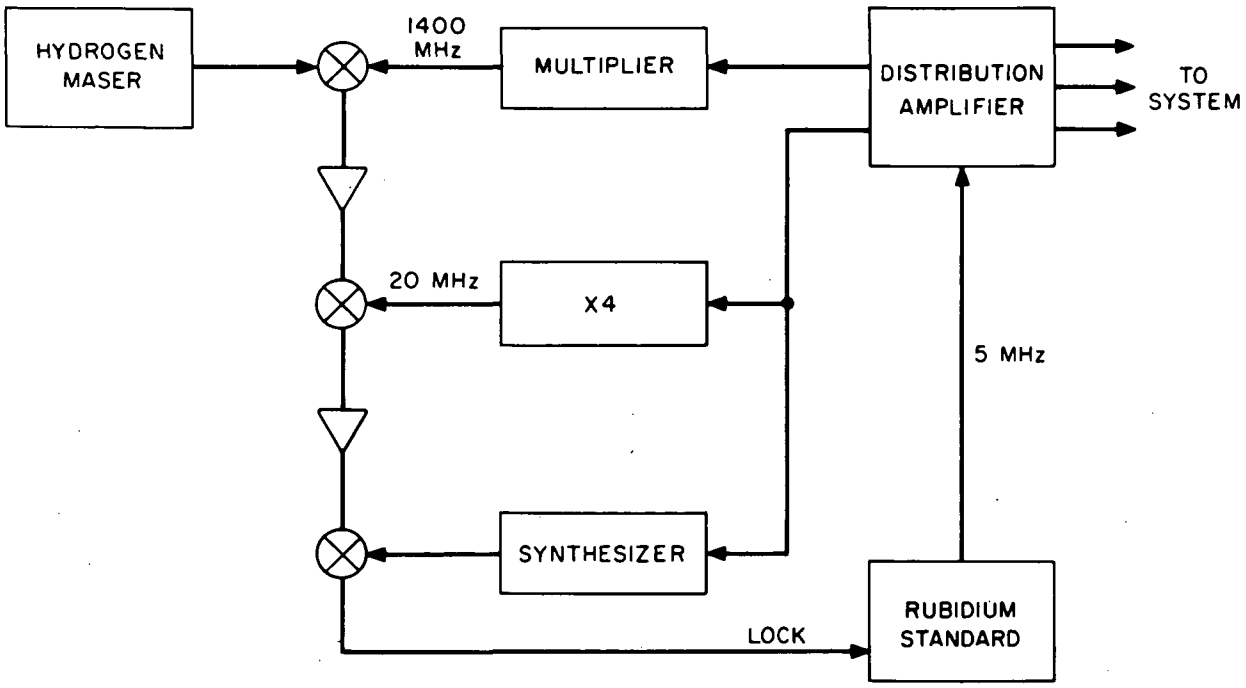

Figure 8. Hydrogen-maser frequency reference system used in VLBI observations at Agassiz.

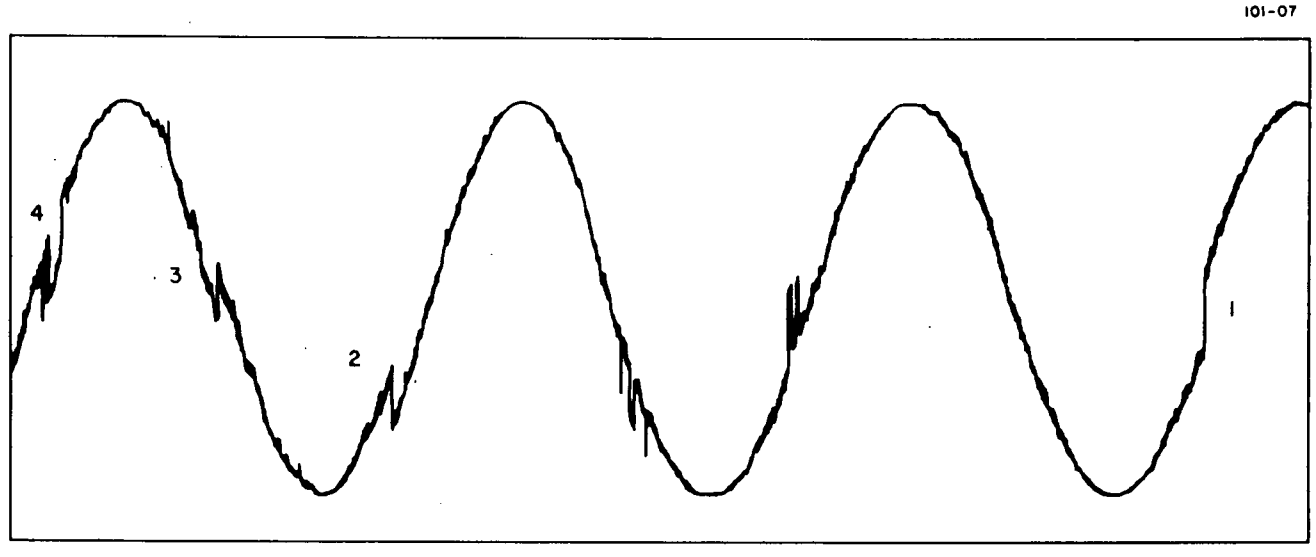

Figure 9. Video-converter output (1 Hz) showing phase jumps (1, 2, 3, and 4) and jitter before system changes. Plot produced under the test conditions shown in Figure 7.

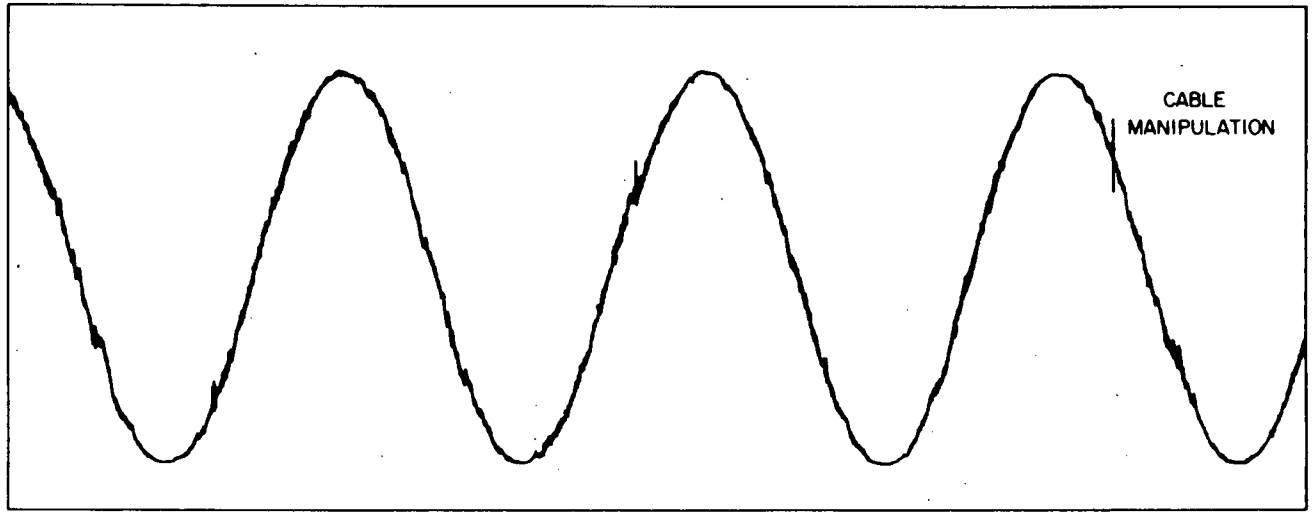

Figure 10. Video-converter output (1 Hz) showing improvement in phase stability following system changes. Momentary phase excursion caused by severe cable movement is shown.

considered imperative that such a check be made at OVRO in preparation for any future work. Similar tests made at Haystack by other observers [9] have demonstrated the phase performance of that station.

3.3.2 System sensitivity

Two methods were used for determining system sensitivity: standard Y-substitution noise-tube injection and total-power observations of sources of known strength. The system temperatures determined from the former are given in Table 4. Such tests were made periodically throughout the sessions. At L-band, the OVRO system produced the total-power readings summarized in Table 5.

3.3.3 Frequency and time-synchronization tests

Both the maser at Agassiz and that at Haystack have been extensively documented regarding their frequency and phase stability [10]. The Rb standard used during two sessions at Agassiz has been checked against the SAO maser and shown to have short-term stability of 8 parts in 10^{13} over 83-sec averaging time. The OVRO Rb standard was not documented as regards its stability; however, it had been used in a previous VLBI session between Goldstone and NRAO and was expected to be stable within 2 parts in 10^{12} (100-sec averaging).

Appropriate time synchronization between Agassiz and OVRO was attained by mutual adherence to UTC (USNO) time. This was set at OVRO by portable Rb and portable cesium clock trips to the Pt. Mugu Time Standards Laboratory and the Goldstone Time and Frequency Laboratory and maintained by Loran C reception from Dana Pt., Indiana. At Agassiz, East Coast Loran chain reception and portable crystal-clock checks with the SAO master clock were used to set the VLBI station clock. Synchronization between Agassiz and Haystack was maintained with frequent comparisons by means of the portable crystal clock.

Table 5. Representative total-power measurements at OVRO.

Source	Measured values		Calculated source strength (f.u.)	Published source strength (f.u.)
	ΔT (K)	Ratio S_n/S_{3C273}		
P 1127	—	0.15	—	—
3C279	4.5	0.23, 0.27	8.3, 10.5	11
3C84	4.8	0.49	11.0	12
W_3OH	14.3	0.94	33	—
3C273	14.3	1.00	32.4	31
3C147.1	15.5	1.08	35	—
Orion	81	5.7	184	360
100°K cal	100	7.1	230	—

Because the recording frame period (16, 800 μsec) was an integral multiple of 100 μsec, the time presentation at each station, once time was set, would remain constant in the last two digits (tens and units of μsec) as long as neither the time accumulator nor the video-frame generator malfunctioned. In a limited fashion, therefore, the constancy of these digits was a partial check on the timing-system performance.

3. 3. 4 Pointing tests

Drift scans were made at each dish to confirm its beamwidth and pointing accuracy. In general, total-power measurements were made as the source drifted through the beam, which had been positioned several seconds ahead of the source's path and stopped.

3. 3. 5 Sky frequency and IF bandwidth determination

To determine the position of the desired sky frequency within the IF and video channels and the shape of their bandpass characteristic, RF sweep-frequency tests were made at both OVRO and Agassiz. At OVRO, an RF sweep generator feeding a $\lambda/4$ stub antenna was used to inject a signal at the near field of the antenna. The swept signal, with markers, was passed by the RF, IF, and video stages, then detected and plotted against frequency. Results of this test showed that the sky frequency was centered in the IF band and that the experiment frequency was centrally located in the 350-kHz-wide video passband of the converter unit. At Agassiz, basically the same test was made, except the RF sweep signal was injected into the feed via a pad. A plot of the IF band, which shows the characteristic double-humped response of the OVRO L-band paramp, is given in Figure 11.

3. 3. 6 Simulated correlation experiment

To determine the proper operation of the video and recording systems and to establish the operating threshold of the SAO VLBI system, a simulated correlation experiment was made. In this test, the equipment was arranged

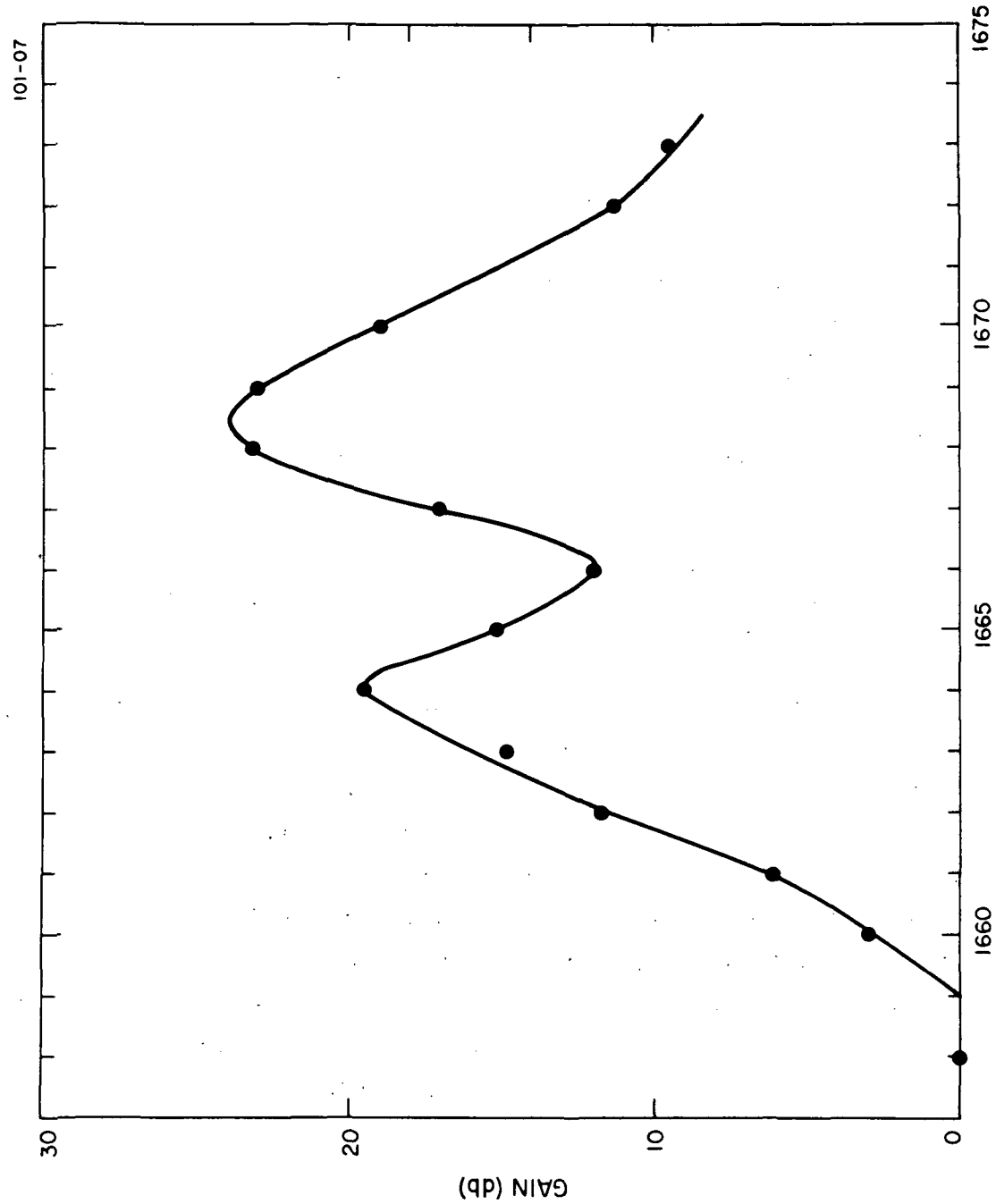

Figure 11. Response characteristic of the OVRO L-band paramp and feed.

as shown in Figure 12 with a variable common noise-signal source and independent noise background sources. Various ratios of (S + N)/N were recorded, and the digital records were processed to determine the record length necessary for fringe detection. These runs are summarized in Table 6, which also gives representative (S + N)/N values for several natural sources over the Agassiz–OVRO baseline. Integration over 50 digital records (10 sec) was sufficient to reveal fringes down to $S/N \approx 0.01$.

3.3.7 Performance verification through ATS 5 observations

Because the ATS 5 signal received over the Agassiz–OVRO baseline was modulated in several known formats, detailed evaluation of the signal was useful as a check on system performance. Joint system sensitivity, response flatness, RF center frequency, and bandpass widths were all determined by study of the frequency spectrums of the correlation functions. The results of these measurements are discussed in detail in Section 5.

3.4 Recommended Improvements in Preobservation Testing and Signal-Processing Hardware

An important preparation to be made at each terminal of a VLBI baseline before observations is the determination of reasonable phase stability in its RF, local-oscillator, and frequency-standard elements. Appropriate tests are described in Section 3.3.1. Test methods used previously, however, were cumbersome and required two digital frequency synthesizers for the phase locking of the RF test signal, one being an expensive 500-MHz unit. To simplify this test arrangement, a microwave synchronizer has been obtained; it permits direct phase locking of the test signal to the frequency standard. This compaction of equipment will simplify the field testing of the antenna/receiver system and the determination of the effect of the frequency standard on overall phase performance.

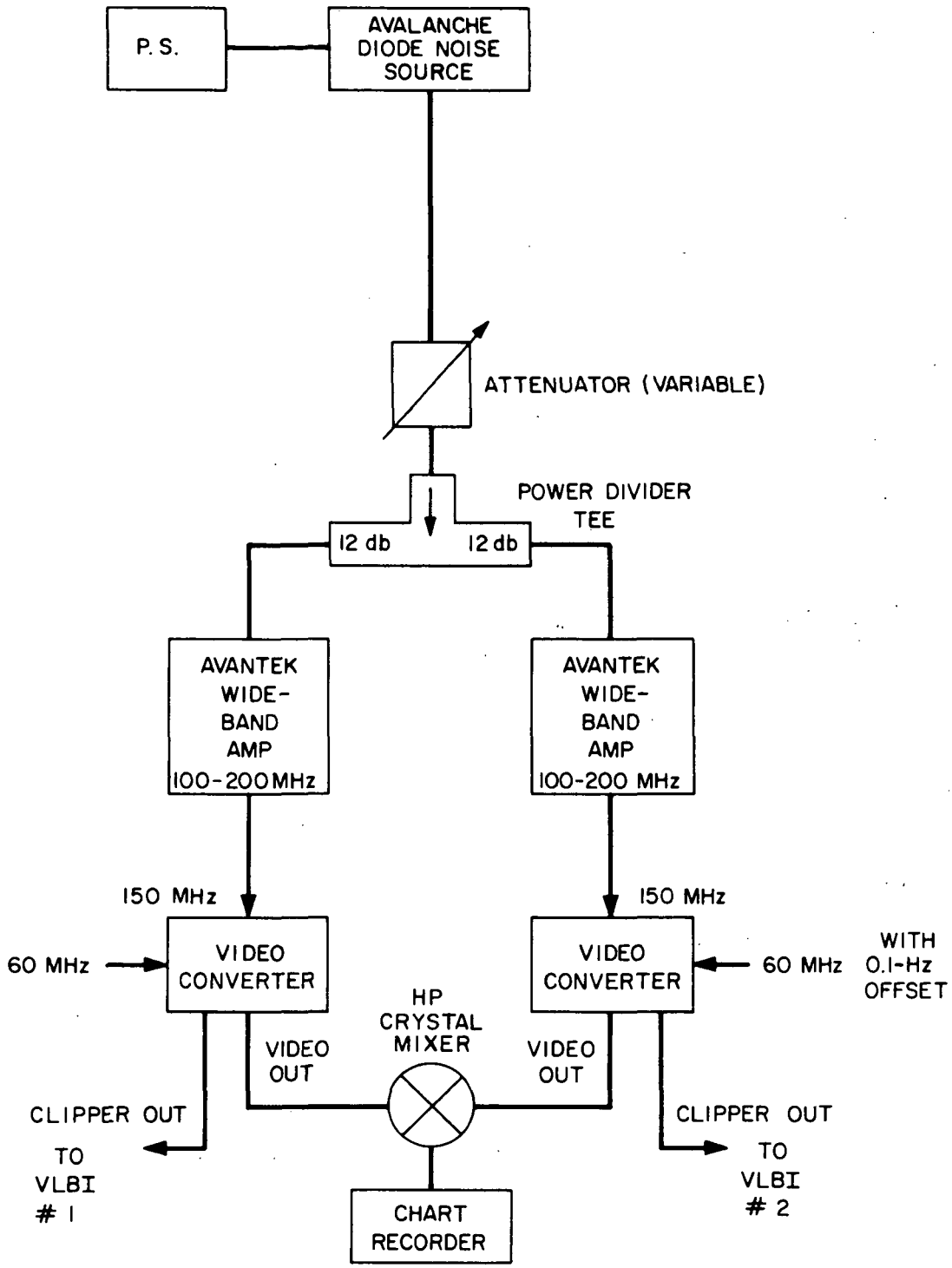

Figure 12. Test arrangement for common-input, simulated correlation experiment.

Table 6. Summary of test conditions for simulated correlation test.

Pad value (db)	Video output $\left(\frac{S+N}{N}\right)_{power}$	Expected correlation at L-band $\left(\frac{S+N}{N}\right)_{power}$	
0	1.109		
3	1.054		
6	1.026	1.0175	3C273 (OVRO—Agassiz)*
9	1.0135		
13	1.0061	1.0058	3C279 (OVRO—Agassiz)*

*Calculated joint-station ratio.

A second essential test is the thorough checking of all frequency standards used in the VLBI program to ensure frequency and phase stability. These tests should be made against each other and in comparison with a master reference, preferably a hydrogen maser. Spectral analysis or averaged period measurements with resolution to 10^{-14} should be employed.

The following instrumental changes, in order of decreasing desirability, are recommended to improve both processing performance and field reliability.

1. Improved reel-to-reel interchangeability between the several VR660 video tape recorders used as field recorders and in data playback processing. At present, tapes made on one recorder cannot be played back on another without loss of playback synchronization and excessive bit errors. Consequently, data tapes cannot now be processed routinely at a central playback facility but must instead await shipment of the field recorder to the playback site. Three partial approaches can be considered to permit reel-to-reel interchangeability:

   a) Flywheel control in the playback electronics of the asynchronous data pulses from the video tape recorder. This would limit the insertion of extraneous noise pulses into the digital record.
   b) Modification of head and capstan servo electronics to permit greater range of control over tape-head tracking.
   c) Closer control over video-recorder model type and performance characteristics. At present, the interchangeability problem is greatest between a model VR660-C and a VR660-B converted to "C" specifications. Presumably, two Model VR660-C's would have beter compatibility.

2. Battery backup for all clocks and frequency standards. At present, it is usual to provide instantaneous battery backup for the station frequency standards in the event of line-power failure. However, the clock accumulators are not protected in this way and require, especially at remote sites, a difficult and time-consuming resetting after line outages. A recommended improvement would be a battery pack unit of 10-hour capacity for both standard and clock at each station.

3. Rubidium portable clock. To facilitate time sets at remote sites where Loran C reception is not adequate for precise setting, a small, lightweight Rb portable such as the GTC Model 307A is very useful. It can provide direct synchronization between VLBI sites and sites with local time standards traceable to a common epoch. At present, SAO is fitting a GTC 307A for 14-hour battery life.

4. Distribution amplifiers for standard frequencies. In order to provide signals to the elements of the VLBI system as well as to various synthesizers used in the test described in Section 3, distribution amplifiers are needed. In addition to the elimination of the loading of the frequency standard, isolation between various units is essential. The phase-stability testing described in Section 3 showed that the 1-MHz clock-drive input must be isolated from the video-converter 1-MHz local-oscillator reference input. In addition, the 5-MHz reference to the maser chain (Figure 8) must be isolated from the 5-MHz drive to the data sampler (used when the sampling rate is 714 kbits/sec).

5. Improved RFI and power-line transient immunity for the VLBI system clock. At times, the susceptibility of these clocks to extraneous signals has caused clock jumps. Power-line filters would probably be a partial answer. System power regulation could also be improved.

6. Aids to editing the video tape during playback digital processing. At present, the video playback system incorporates an incomplete automatic playback capability by which preset time entries control the start and stop of the playback process with 1-sec resolution. Completion of this feature would permit easier editing of tape records, especially if the records are closely spaced on the tape. Another editing aid in playback, particularly when coarsely searching the video tape, would be an improved time channel that uses one or both of the auxiliary audio tape channels. Currently, only verbal time cues are given; radio voice announcements (e. g. , CHU) or a time code presentation (and readout) would be superior.

7. Synchronization of the video frame rate with the delayed 1-pps clock output. This modification would serve three purposes:

a) It would provide a check of the time code presentation every second.

b) At the 720-kbit/sec sampling rate, it could provide digital records with the identical start time as those taken on a Mk I system, when the automatic start feature described in 6 above is available and used.

c) It would provide precisely coincident data frames from the two or more stations producing tapes.

4. DATA REDUCTION

4.1 Data Reformating Modifications

Over 25 hours of video tape (at 714 kbits/sec) were recorded at each station during the three observing periods. During the first period, 433 3-min and 5-min runs were made. Approximately 100 runs were completed in the second period, and 36 in the third.

With the first digital tapes produced according to the procedure shown in Figure 13a, we began to test the preprocessing program that had been previously written to reformat the data and convert from 9-track to 7-track tape [3]. As adjustments were made to the playback unit during the checkout procedure, some changes in the data-processing scheme became necessary.

One of the primary functions of the preprocessing program is to standardize the variable record and segment lengths caused by data loss during the head-switching interval. The digital tape produced by the SAO back end contains approximately 0.2 sec of data in each physical record. Logically, each record consists of 12 blocks of data for 1/60 sec each, with every block also containing a 9-byte time code, a section of "garbage" produced during the head switching on the video tape, and a 10-byte synch word. Part of every thirteenth block is dropped so that an interrecord gap can be written on the tape. The number of bytes in the section of garbage is a variable ($8 \pm n$; $n \leq 4$) to allow the video tape and the digital to be constantly kept in time alignment during the playback. This fact presents a problem for the data processing, as each block representing 1/60 sec of data has $2000 \pm n$ bytes, rather than exactly 2000. Thus, the 12 blocks in the physical record have $24,000 \pm 12n$ bytes. The physical record length of the tape is forced to a maximum value so that the length will be a constant for data processing. The tape is 9-track, but each byte contains only 6 bits of information, rather than the usual 8, so that it can later be transcribed onto 7-track tape.

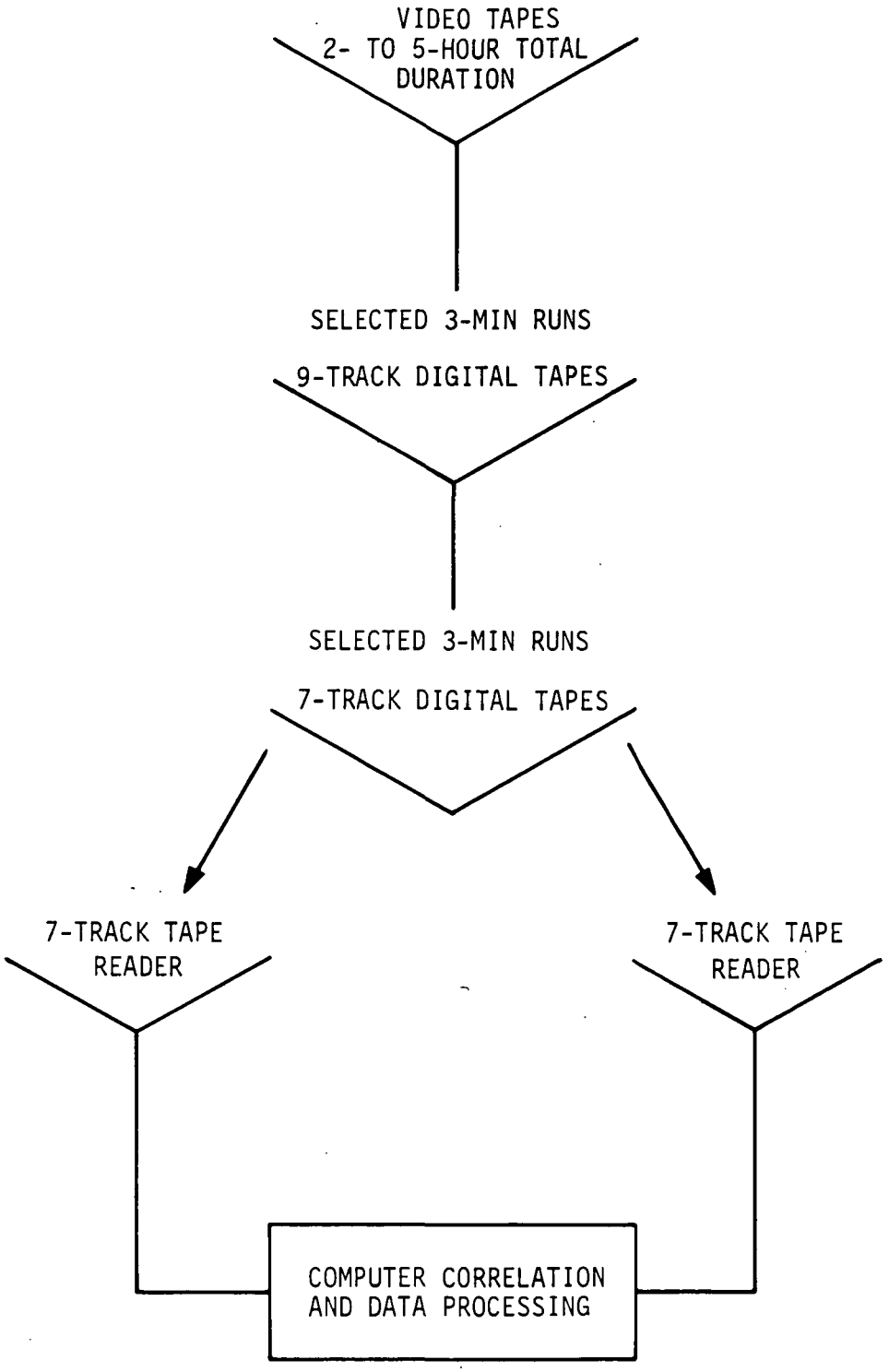

Figure 13a. Video-tape reformating procedure. Two reformating steps are required — from video to 9-track and from 9-track to 7-track tape.

One section of the program counts the number of bytes written during the head switching in each of the logical blocks and replaces them with exactly 8 bytes. The next piece of data (the first byte in the synch word) is then placed at the beginning of a computer word in memory. The resultant physical record is exactly 24,000 bytes or 2400 computer words long and corresponds to exactly 0.2 sec of data. This standard record can then be processed by the fringe program with a minimum of adjustment.

During the checkout of the unit, it was found that the occurrence of the head-switching intervals could not be so closely controlled as anticipated. Consequently, the mean placement of the head-switching point had to be planned about 32 bytes earlier in the data, so that deviation from the mean by as much as 32 bytes would not result in the synch word of the next segment being disturbed (Figure 13b).

4.2 Baseline-Determination Procedure

The determination of the baseline parameters and celestial coordinates by VLBI observations requires the collection and processing of a large amount of data. The most precise information is contained in the phase of the fringes. However, it is very difficult to identify one particular fringe out of several million. It is easier and quicker to measure the delay and the fringe rate. Of these two, delay mapping is more precise [11]; therefore, a method has been developed to recover baseline parameters from delay measurements. Basically, the method requires the observation of at least three celestial sources, each at three different times. The following method of processing the data is independent of the size of the error and yields baseline errors, source-position errors, and clock offset errors independently, without use of a "bootstrap" type of iteration technique.

Let D, δ_B, H_B, δ_s, and H_s be the assumed parameters of the baseline and source, respectively (as in equation (1)). Let the errors in these parameters be ΔD, $\Delta\delta_B$, ΔH_B, $\Delta\delta_s$, and ΔH_s, and let the clock offset error be ΔT. Then the difference between the assumed delay τ_g and the delay

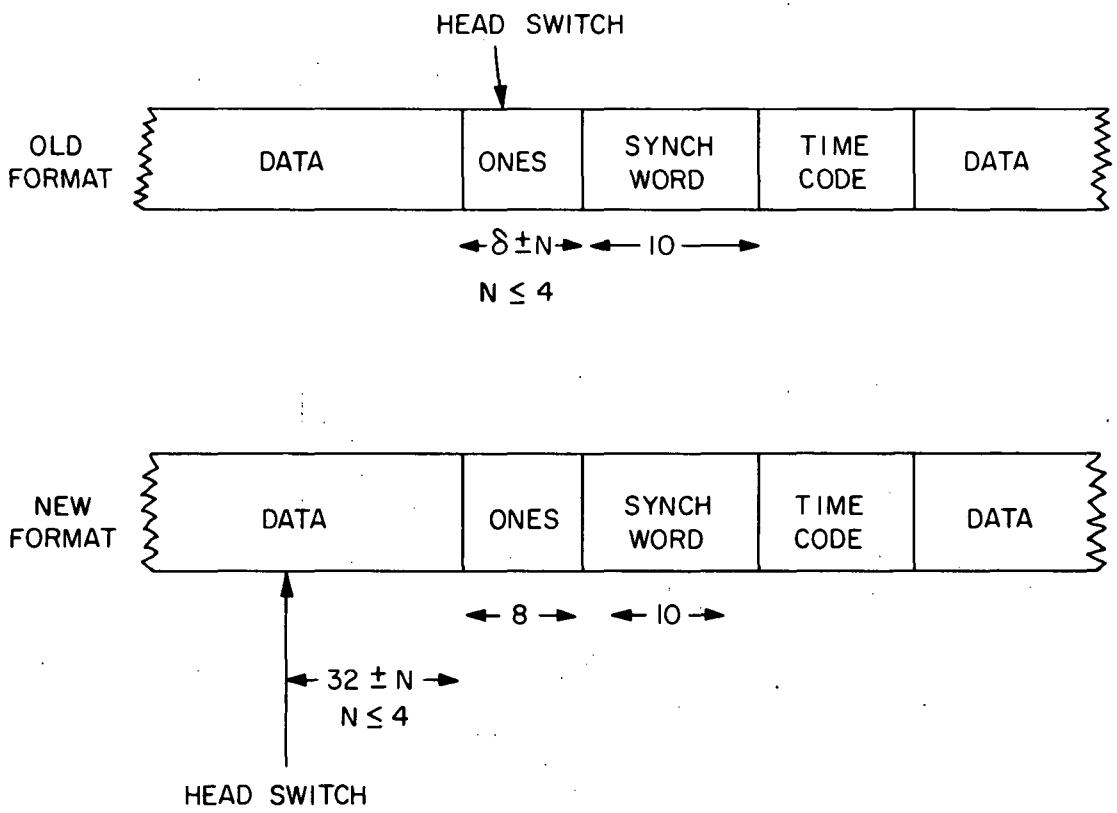

Figure 13b. Old and new video tape formats showing changed head-switch location relative to the code blocks.

measured by the fringe reduction program τ_m is of the form

$$c\,\Delta\tau = A_0 + A_1 \cos H_s + A_2 \sin H_s \quad , \tag{1}$$

where

$$A_0 = c\,\Delta T + (D - \Delta D) \sin (\delta_s - \Delta\delta_s) \sin (\delta_B - \Delta\delta_B)$$

$$- D \sin \delta_s \sin \delta_B \quad , \tag{2}$$

$$A_1 = (D - \Delta D) \cos (\delta_s - \Delta\delta_s) \cos (\delta_B - \Delta\delta_B) \cos (H_B - \Delta H_B + \Delta H_s)$$

$$- D \cos \delta_s \cos \delta_B \cos H \quad , \tag{3}$$

$$A_2 = (D - \Delta D) \cos (\delta_s - \Delta\delta_s) \cos (\delta_B - \Delta\delta_B) \sin (H_B - \Delta H_B + \Delta H_s)$$

$$- D \cos \delta_s \cos \delta_B \sin H_B \quad , \tag{4}$$

where the measured quantity is $\Delta\tau$. By making three observations on a source (at three different values of H_s), we can obtain the values of A_0, A_1, and A_2 for that source. Equations (2), (3), and (4) can then be used to eliminate the unknown errors associated with the source ($\Delta\delta_s$, ΔH_s), and we obtain an equation of the form

$$x + k_1 y + k_2 z = k_1^2 \quad , \tag{5}$$

where

$$k_1 = A_0 + D \sin \delta_s \sin \delta_B \quad ,$$

$$k_2 = (A_1 + D \cos \delta_s \cos \delta_B \cos H_B)^2 + (A_2 + D \cos \delta_s \cos \delta_B \sin H_B)^2 \quad , \tag{6}$$

and

$$x = (D - \Delta D)^2 \sin^2 (\delta_B - \Delta\delta_B) - c^2 \Delta T^2 \quad ,$$

$$y = 2c \Delta T \quad , \tag{7}$$

$$z = \tan^2 (\delta_B - \Delta\delta_B) \quad .$$

For each source, k_1 and k_2 can be determined by three observations since they involve only A_0, A_1, and A_2 and the assumed parameters. By using a minimum of three sources, three equations of the form (5) can be generated, from which x, y, and z can be recovered. This leads to the values of ΔD, $\Delta\delta_B$, and ΔT. From equations (2), (3), and (4), $\Delta\delta_s$ and $(\Delta H_B - \Delta H_s)$ can then be recovered for each source.

4.3 Postprocessor Development

A computer program was developed that uses the technique described above to find the baseline and source parameters and the clock offset error. In practice, greater accuracy will be achieved by observing many sources, each many times, and solving the overdetermined system of equations that results by applying least-squares-fitting procedures. It is assumed that corrections for atmospheric delay are either negligible compared to the accuracy of $\Delta\tau$ measurement or known. It is also assumed that the declination and polar axes of the antennas intersect. If this is not so, a declination-dependent term appears that can be taken care of by observing additional sources. In principle, the technique can be used for absolute determination of source, baseline, and clock offset parameters without recourse to approximations. The variances of measured quantities will depend on the variance of $\Delta\tau$. This in turn depends on the bandwidth of the system, the signal-to-noise ratio, and the integration time.

During this contract period, a first version of the postprocessing program was written, debugged, and successfully tested. One subroutine determines by least-squares fitting the best estimate of three independent variables

from a set of more than three linear, independent equations involving those variables. This routine is called by the postprocessor driver program to form a least-squares estimate of two sets of parameters cited in the equations developed above. A, B, and C are determined by observing one source at three or more different times of day; and x, y, and z are determined by observing three or more different sources. The final result of the program is estimates of the error in assumed baseline length, baseline declination, time-delay offset, source declination, and source hour angle relative to the baseline.

An input routine for the postprocessor driver accepts the identification codes of the two ground stations, the source, the date, the time of the observation, and the time delay, which is to be found by processing the fringes. Arrays are dimensioned so that up to 10 observations of each of 10 sources can be made — a total of up to 100 data cards per baseline computation.

4.4 Fringe Processing Program

Additional modifications to the fringe processing program were performed during this period. The most important of these was a reorganization of the looping procedure so that each digital record of 0.2 sec of data would be broken into 12 segments of 1/60 sec each, rather than the 10 segments of 0.02 sec each used in the original program. Phase information is calculated for each segment so that the phase-correction calculation is no longer needed. This change to 12 segments was necessitated by the formating of the SAO tapes based on the video recorder's frame size, which corresponds to 1/60 sec of data between each head switch.

Subroutine CORREL, the correlation program, was also modified so that instead of shifting the two records one bit at a time for each successive correlation, they can be shifted by n bits between correlations. This feature is sometimes used to reduce computing time by performing "coarse" searches during preliminary phases of the data reduction.

4.5 Summary of VLBI Computer Programs

The summary below lists and describes the computer programs used for data processing and analysis. The programs are listed in the order in which they would ordinarily be used. All were written for the CDC 6400.

VISIB: Subroutines: STAR
Language: Fortran IV

Given two station locations to specify a baseline, this program will produce a line printer plot showing the times for which a source is visible from both stations on a given date. A plot is produced for each limiting elevation angle specified. Each plot may include up to 20 sources.

EPHEMB:

This program is available on tape at SAO. It produces a series of positions for artificial sources such as ATS 5 for the dates and times specified.

SCHED: Subroutines: LOC, HMS, MOVE, DECL
Language: Fortran IV

SCHED produces an observing schedule for each day of an experiment. The date, source names and positions, and station names and positions are specified, along with the start time in Universal Time and the source for each observation. A schedule is printed in local time for each station, showing pointing angles for the sources. For the offset station, synthesizer settings are also calculated and printed. Checks are made to be sure that adequate slewing time has been allowed to move the dish between observations and that the physical tracking limits at Agassiz have not been exceeded.

TAPES: Subroutines: IO-IO, DECTIME, PRESS
Language: Fortran IV and Compass

The 9-track tapes produced from the video tape by the SAO playback equipment are reformated and converted to 7-track by this program. A 7-track tape with a fixed record length of 2400 words is produced, along with a printout of four key words from each record and the time for each record in

hours, minutes, and seconds (to 1 μsec). The key words enable the user to check the reliability of the information on the original 9-track tape and to locate any record splitting or excessive drifting that may have occurred during the playback operation.

VLBI 1: Subroutines: READGH, PLOT2V, CORREL
Language: Fortran IV and Compass

This program performs the correlation of the two tapes, one from each station, for data from natural sources. One of the bit strings is shifted by a calculated delay, and a search is made over a range of fringe frequencies to find the peak of the correlation function. A plot of the fringe amplitude versus delay is produced for each fringe frequency.

VLBI 2: Subroutines: READGH, FOURIER, PLOTIN, CORREL
Language: Fortran IV and Compass

This program is a version of VLBI 1, modified to handle data from artificial sources such as ATS 5. A record or a segment of a record from one tape may be correlated against a number of consecutive records from the other. A Fourier-transform program to obtain fringe intensity as a function of fringe frequency is included.

POSTPR: Subroutines: INPUT, LSTSQR, SOMSQR, INSERT, DETERM, OUTPUT
Language: Fortran IV

With data from up to 10 observations as input, this postprocessing program calculates a least-squares estimate from an overdetermined set of equations. The inputs are source locations and $\Delta\tau$'s (measured minus computed delay) from VLBI 1, and the outputs are corrected baseline length and orientation, source locations, and $\Delta\tau$'s for each observation.

5. DISCUSSION OF RESULTS

5.1 Results on Natural Radio Sources

5.1.1 Short baseline observations

Observations of several extragalactic sources were made on the Agassiz–Haystack baseline during three sessions. Linear polarization was used, and various combinations of rubidium and hydrogen-maser frequency standards were employed at the two terminals.

Fringes were observed on two of the three sessions, the middle session being unsuccessful because of an error in setting the maser control loop. The sources that produced fringes were 3C84, 3C147, 3C273, 3C279, and 3C286. Of the 17 runs processed, 14 produced fringes.

Typical correlation functions plotted as a function of delay are shown in Figures 14a, b, c, and d for 3C273, 3C286, 3C147, and 3C84. The correlations in these cases were performed over 100 records, and the actual integration time was 9.58 sec. It is seen that the peak of the correlation in Figure 14a does not occur at the expected point in delay ($\tau = \tau_g$); it occurs approximately 2.8 μsec to the right. This offset is the difference between the measured and the calculated delays in the data-reduction section.

In most cases of data processing, the search parameters used were 30 points in delay (corresponding to 42 μsec) and 20 points in fringe rate at 0.01-Hz intervals. When integration longer than 100 records was needed, the fringe-rate interval was changed appropriately. Typical computer running time for such a run was 150 sec. The running time depends somewhat on the instrumental delay, as discussed in Section 4.

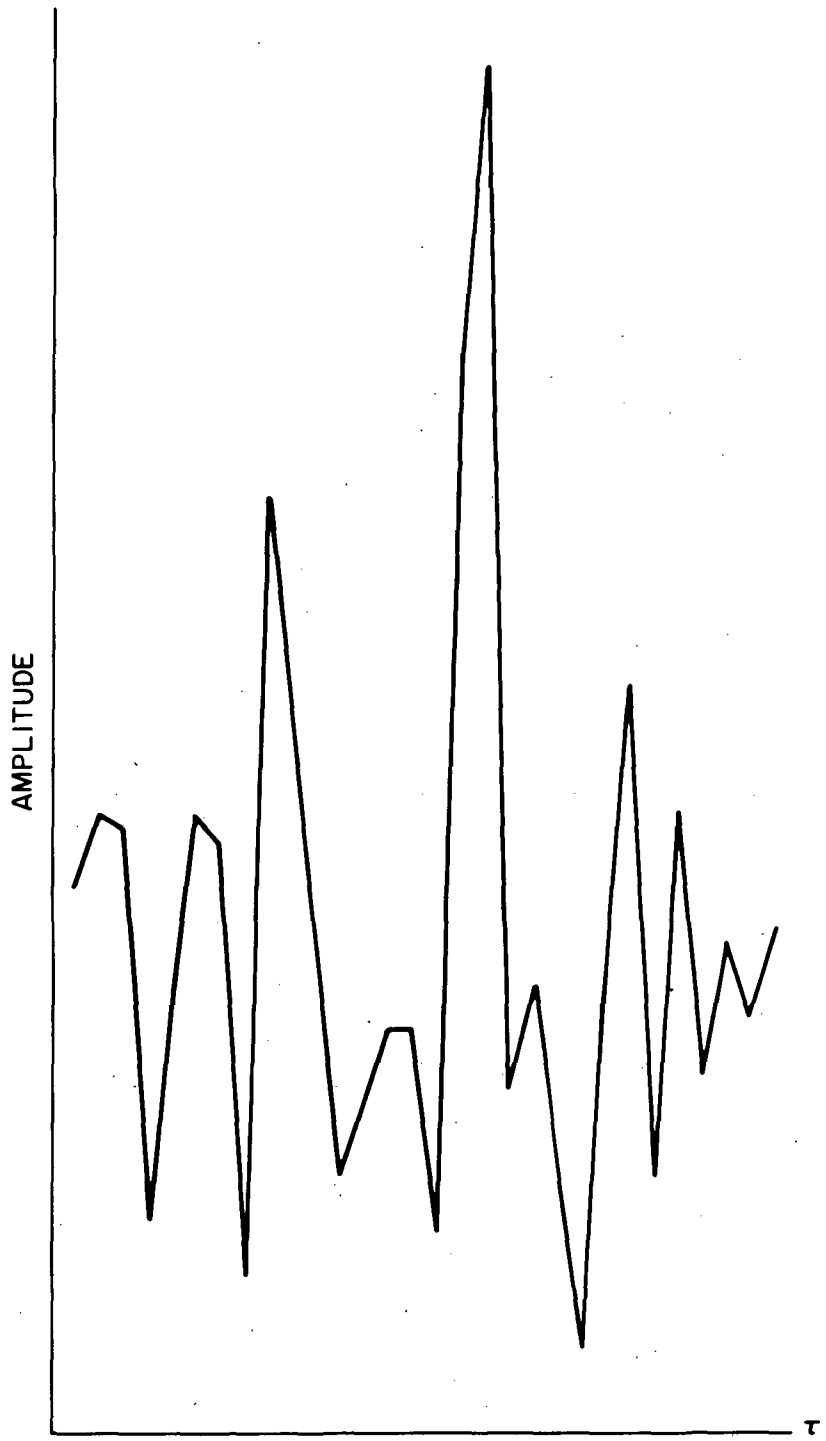

Figure 14a. Correlation function for quasi-stellar source 3C273 over the Agassiz–Haystack baseline.

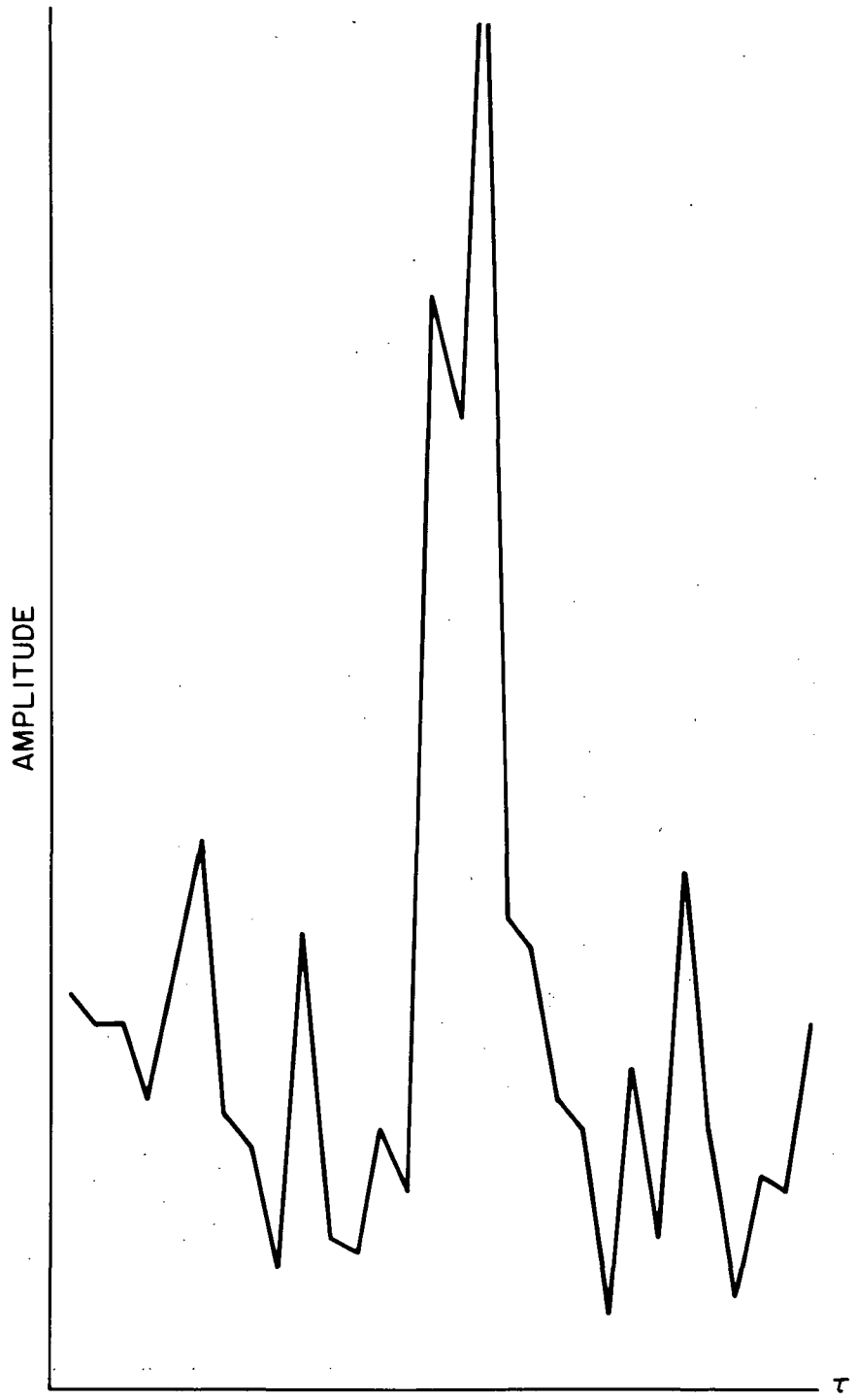

Figure 14b. Correlation function for source 3C286 over Agassiz–Haystack baseline.

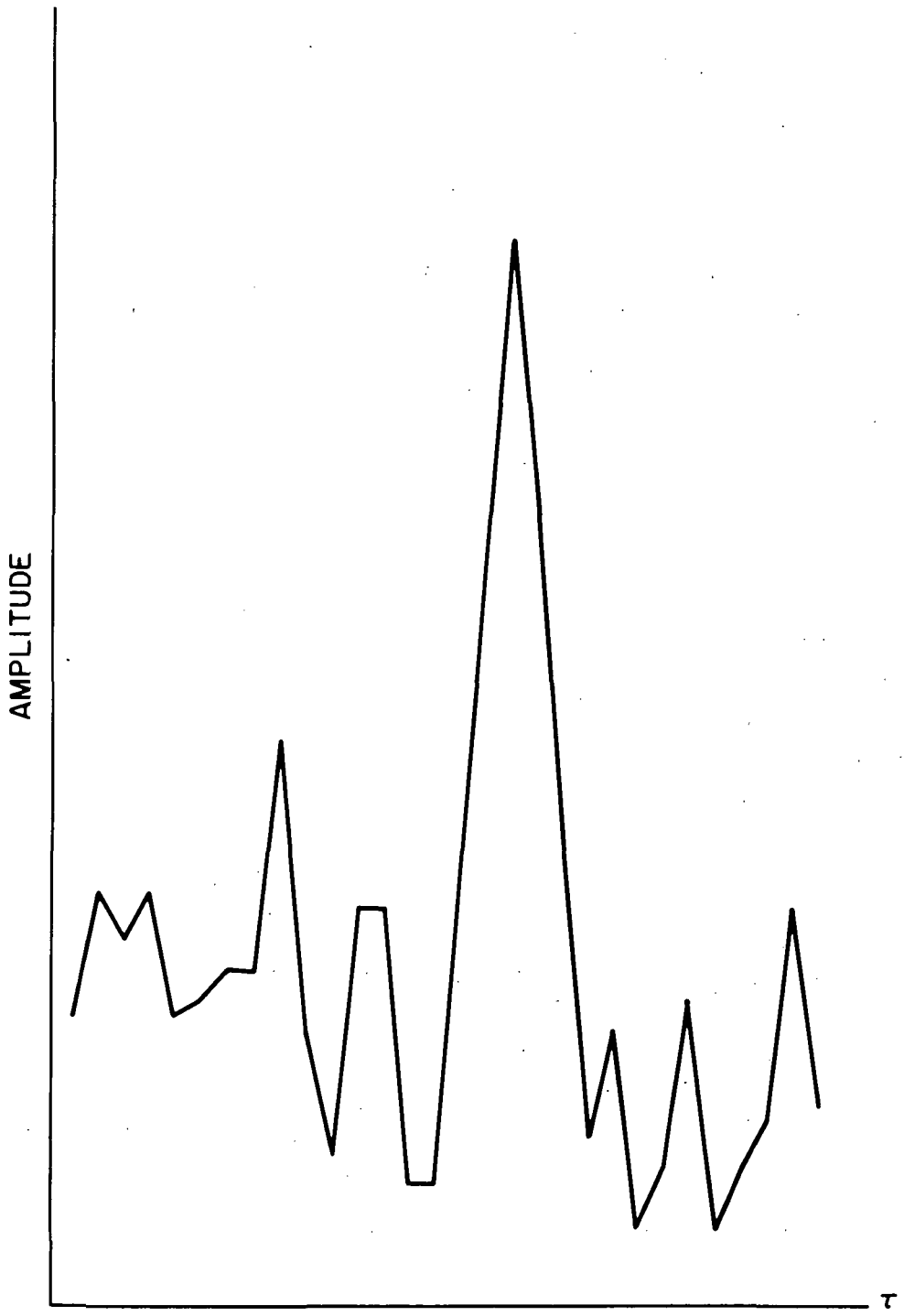

Figure 14c. Correlation function for source 3C147 over Agassiz–Haystack baseline.

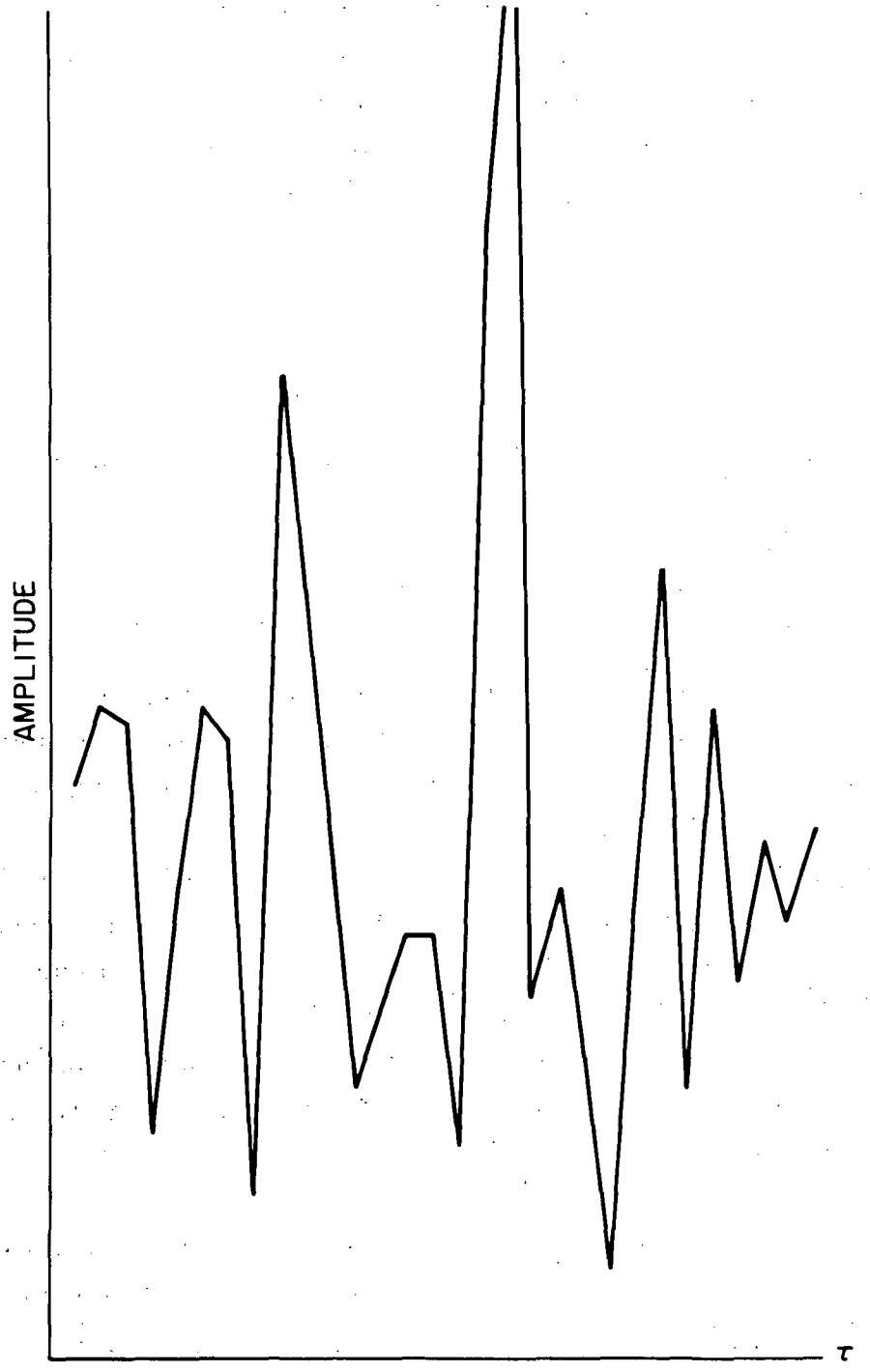

Figure 14d. Correlation function for source 3C84 over Agassiz–Haystack baseline.

By use of data from 3C279, 3C147, 3C286, and 3C273, as tabulated in Table 7, a baseline solution was attempted. This solution was calculated on the basis of time delays prepared by curve-fitting interpolations in the delay domain. The results of this solution were not satisfactory and are not given here, because the interpolations were too coarse. For several runs, a finer estimate of the delay time was made by taking the slope of the power spectrum phase

$$\Delta\tau = \frac{\Delta\phi}{\Delta f} \quad ,$$

but a sufficient number of points was not obtained for a new solution to be made.

5.1.2 Long-baseline observations

Of the two sets of experimental data recorded over the Agassiz–OVRO baseline, limited processing was done on the data collected at C-band in November–December 1969, and a more detailed search for fringes was made on the L-band data collected in March 1970. With the C-band data, a fringe search was carried out on observations of 3C273 and 3C454.3. Of the L-band data, the sources 3C273, 3C279, and P 1124-14 and the OH line source in W3 were chosen for fringe search. Since all observations were made at a bandwidth of 360 kHz, the OH line source was possibly very weak. The continuum in W3, though very bright, is not known to have a component sufficiently small so as to be unresolved by the Agassiz–OVRO baseline at L-band. None of these searches yielded fringes.

In view of the results of the simulated test and the short-baseline experiment, as well as the results on the ATS 5 data, it appeared that the lack of success in getting fringes on natural sources on the long baseline between Agassiz and Owens Valley was attributable to one or more of the following causes:

Table 7. Results of VLBI Session 7 (2 August 1970).*

Source	Run	Hour angle	P	D_0	N	$\Delta\tau$	H	sin H	cos H
3C279	7–110	-1.^{h}1939	17	-0.22	30	-3.148	-17.°9085	-0.3074	0.9516
δ = -5.°7351	7–114	0.1437	18	0.243	30	-3.86	2.1555	0.2384	0.9993
	7–118	1.4010	18	0.295	30	-3.787	21.0150	0.3584	0.9336
3C147	7–102	1.8662	17	-0.185	30	-3.059	27.993	0.4695	0.8829
δ = 49.°8395	7–105	2.8869	16	0.053	30	-1.726	43.3035	0.6858	0.7278
	7–107	3.5419	17	-0.187	30	-3.062	53.1285	0.7997	0.6004
3C286	7–104	-5.2859	17	0.405	30	-2.233	-79.2885	-0.9826	0.1857
δ = 30.°6624	7–113	-0.7747	15	-0.438	30	-0.6132	-11.6205	-0.2011	0.9796
	7–117	0.4757	17	0.494	30	-2.1084	7.1355	0.1236	0.9923
	7–120	2.8155	16	-0.306	30	-1.8284	42.2325	0.6717	0.7408
3C273	7–108	-2.9336	15	0.394	30	0.5516	-43.9890	-0.6947	0.7192
δ = 2.°2151	7–109	-1.0109	17	0.207	30	-2.510	-15.1635	-0.2622	0.9650
	7–115	0.8328	28	0.434	50	-3.592	12.492	0.2164	0.9763

*N = Number of delays searched.
P = Position of correlation peak.
D_0 = Doppler peak.
$\Delta\tau$ = Time delay.

1. A possible large clock offset caused by a clock jump resulting from power-line transients.

2. A lack of adequate stability in the phase of the local-oscillator signal.

3. A possible misalignment of the polarizations received at the two terminals.

4. Degraded system performance at C-band.

5. Possible software problems in the calculation of local-oscillator offset frequencies and in the fringe reduction programs.

After each of the above possible causes was checked, it was clear that the inability to detect fringes at C-band over the Owens Valley–Agassiz baseline cannot be attributed to items 3 and 5 above. In fact, subsequent success over the same baseline in correlating ATS 5 signals and in employing natural sources over the Haystack–Agassiz baseline (at L-band) indicates that system techniques and data-reduction methods were not at fault and that the data-recording and playback portions of the instrumentation were operating properly. A large volume of analyses of the circumstances of this experiment and of subsequent system performance tends to narrow the causes of failure to the following, listed in order of probability:

1. Phase discontinuities and/or excessive phase jitter introduced in the RF feed system, local-oscillator system, or frequency standard of one or both of the stations.

2. Gross errors in time synchronization between the stations. Maximum search range in the computer correlation processing was ±50 μsec. Epoch differences greater than this would not normally be discovered, and in such a case, the data would be unusable.

3. Poor receiver sensitivity, coupled with excessive phase jitter as described in (1) above. The lessened sensitivity of the receiver systems at C-band might have resulted in failure to detect the source with integration times on the order of 500 data frames – the number usually employed. This amounted to about a 100-sec integration time, sufficient, under normal conditions, to detect all sources observed.

For the L-band observations of natural sources, only the first possible cause above would appear to apply, because the timing synchronization was quite reliably determined by the ATS 5 satellite VLBI observations and the sensitivity of both antenna systems was established by measurements to be high, as expected at L-band.

The same Rb frequency standard was used in both C- and L-band observation periods at the OVRO terminal. Since this unit had not specifically been tested by SAO, some concern exists that it may have malfunctioned in spite of the fact that it had been employed by other workers in previous VLBI observations that were successful, at least at L-band.

Timing was also weak at OVRO during the C-band observations because of the failure of a portable clock carried from the East Coast terminal. Consequently, dependence on Loran C sky-wave emissions was necessary. This, at best, provided only about ±35-μsec resolution. This situation was markedly improved on the later L-band experiment, mainly because of portable cesium-clock time checks made with the NASA Echo station at Goldstone and a posteriori ATS 5 VLBI measurements.

5.2 Results on the ATS 5 Satellite

5.2.1 Background

During Experiment period IV, observations were made of the geostationary satellite ATS 5 over the Agassiz–OVRO baseline. It was intended that these observations should provide data on the ability to utilize artificial sources for VLBI observations of geodetic quality and on the feasibility of determining satellite position by means of time-delay VLBI techniques. In addition, the strong wide-band signal, variously modulated, was correctly assumed to be useful in assessing system performance, particularly as regards fixing system bandwidth, RF tunability, sensitivity, and time synchronization between the two sites.

Because only two stations were used, no precise measurement of the satellite position was possible; however, it was noted that a locus of α, δ the satellite's angular position coordinates, could be determined from the single baseline. To accomplish this, it was necessary to minimize clock-epoch-alignment errors at two stations and to determine independently the baseline orientation angles, the baseline length, and the satellite range. The first two of these measurements would have been accomplished if the VLBI observations of natural sources had been successful. However, for the reasons given in Section 5.1.2, these natural-source observations did not yield fringes. Consequently, only quantitative estimates of the satellite locus have been calculated by use of a priori values of the baseline parameters and the satellite range and an independent determination of the stations' clock-epoch misalignment based on Loran C data. These position calculations are crude and cannot resolve the satellite motion over the 2-day span of observations.

The most fruitful use of the observations was as a means of checking the operational performance of the SAO VLBI system and of the overall baseline system. Developmentally, it provided a chance to evaluate variously modulated waveforms with different correlation lengths as regards their measurement sensitivity and ambiguity resolution.

5.2.2 Technical summary

The ATS 5 VLBI experiment is shown in Figure 15. The 15-ft L-band Mojave dish transmitted the 25-MHz bandwidth, wide-band frequency translation (WBFT) mode signal to the satellite, which transponded it downlink at 1550.000 MHz to the Agassiz and OVRO dishes, for which satellite pointing coordinates had been calculated. The rotation rate of the satellite and its antenna-beam pattern (with sidelobes) combined to produce at each dish a signal-strength variation that appeared as shown in Figure 16, the period of illumination being 788 msec. The figure also summarizes the data records, in terms of 212-msec long, 152,000-bit digital records, which were processed for fringes for each of the four identifiable modulation modes. The value of the correlation function for each of these records is plotted and illustrates

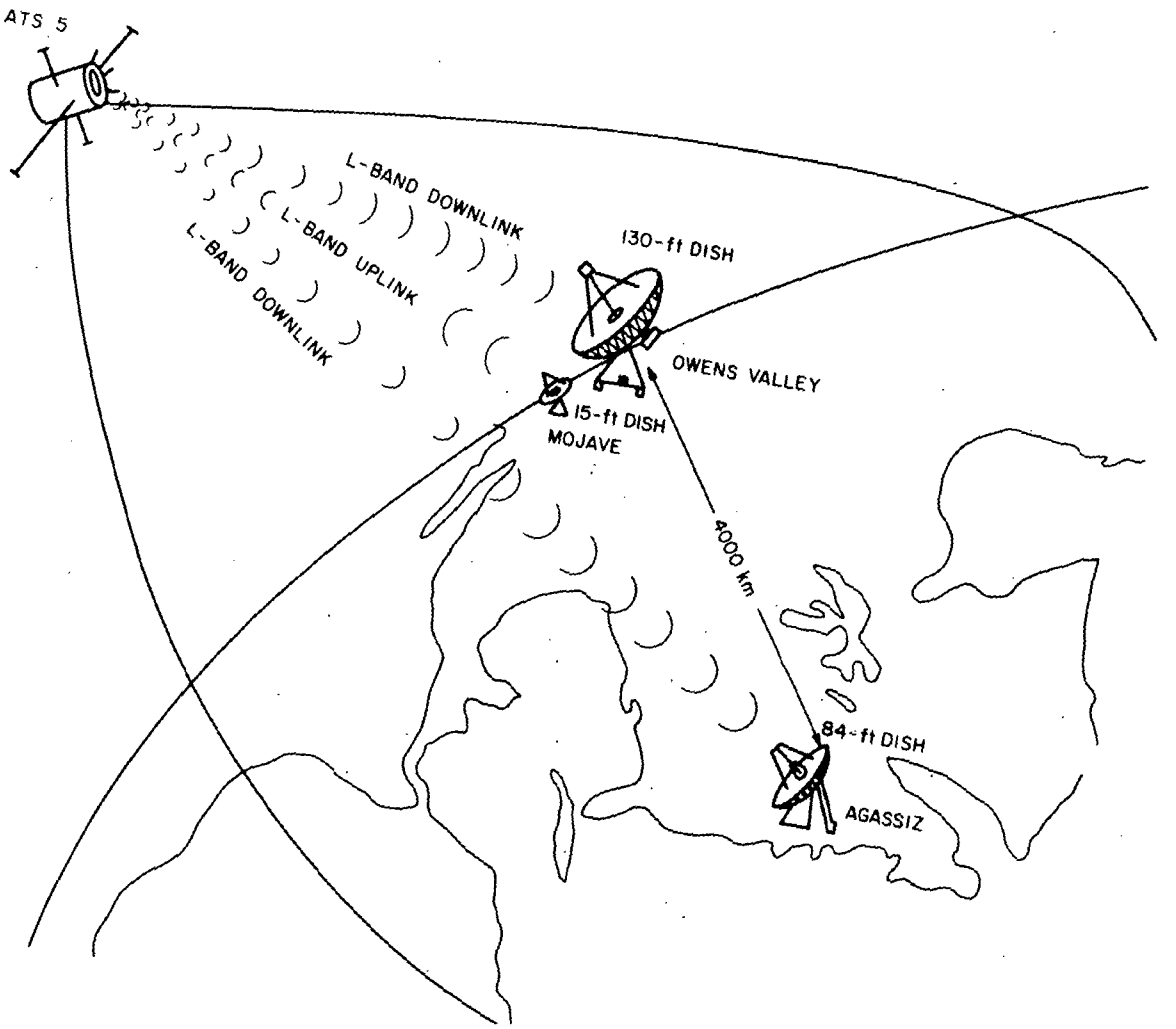

Figure 15. ATS 5 VLBI experiment.

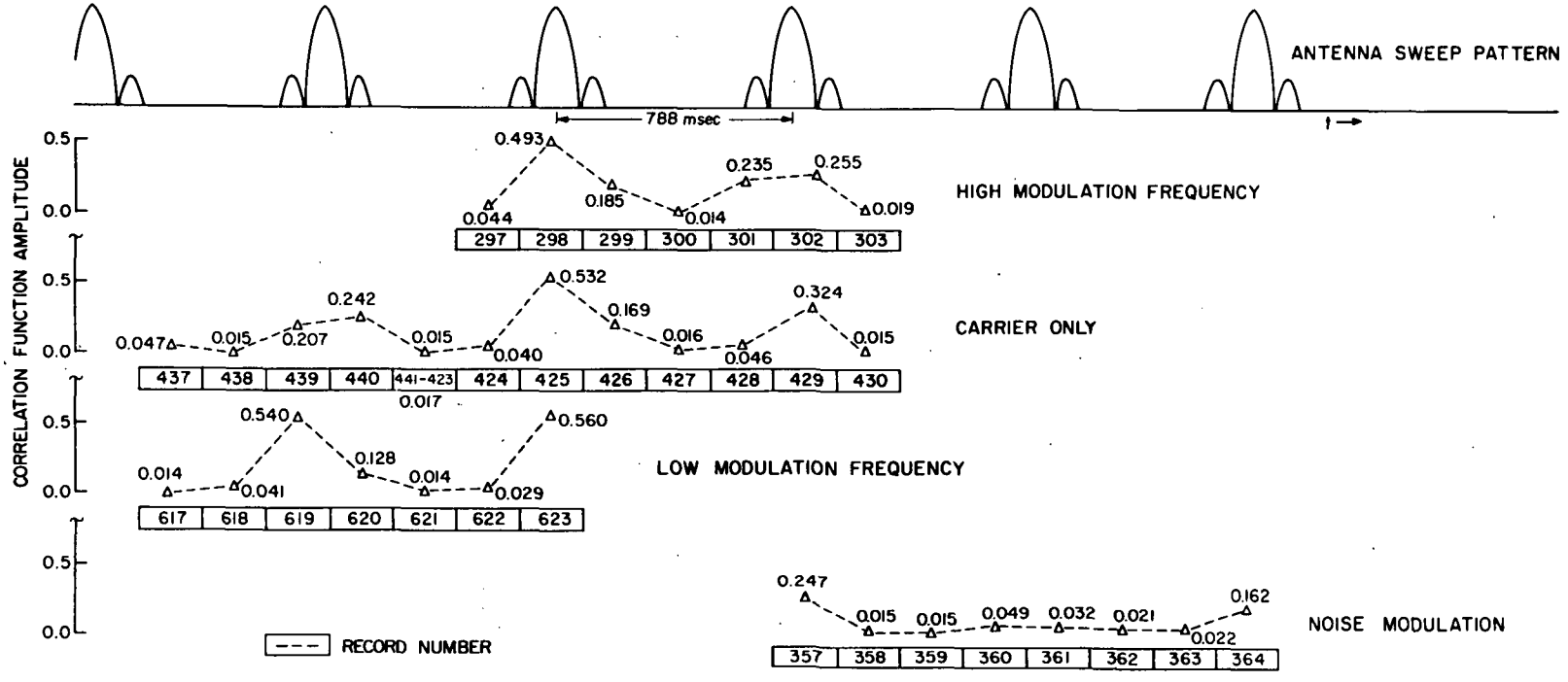

Figure 16. Variation of correlation strength with satellite rotation.

the dependence of the correlation on signal strength, the correlation peaks exactly corresponding to the maxima of the antenna signals.

Since the ATS observations were made without arranging for particular modulation inputs at Mojave, there was no control over the received signal. For the most part, the signal record consists of square-wave PSK modulation at 83.3 kHz, followed by shorter periods of PSK at 8.33 kHz and 833 Hz. Fortunately, several periods of noise modulation amounting to about 30 sec were discovered by means of visual monitoring of the video records by using a TV monitor synched to the frame rate. Correlation analyses were made of a number of representative records of each modulation mode. Figure 16 contains those records of modulation that were fully analyzed.

5.2.3 Signal analysis

As noted above, the square-wave PSK modulation provided a valuable means of checking the frequency and phase response of the correlation system. By evaluating the extensive Fourier products of the several modulation frequencies, a close comparison was made with the predicted theoretical values.

Communications with Applied Information Industries (AII), the controller of the ATS L-band experiment being performed during our observations, indicated that a diode-bridge, balanced modulator was used to produce 0 to 180° phase-shift keying of the L-band carrier. The modulation drive during equipment tests was a square-wave generator, used in both an automatic and a manual sequencing mode (Figure 17a). A PSK modulo-2 data modulator was also employed, at a rate of 1.62 kHz. AII confirmed that both grounded and open modulator input conditions could exist during a transmission sequence, resulting in an unmodulated carrier and a noise-modulated carrier, respectively.

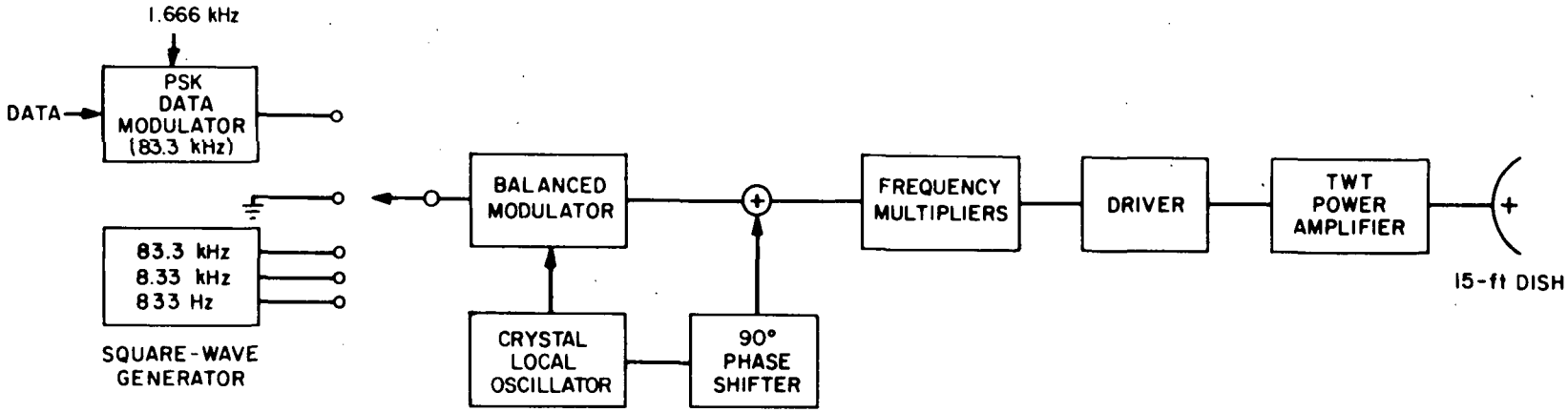

a) MOJAVE PSK TRANSMITTER USING ATS 5
L-BAND WIDE-FREQUENCY TRANSLATION MODE

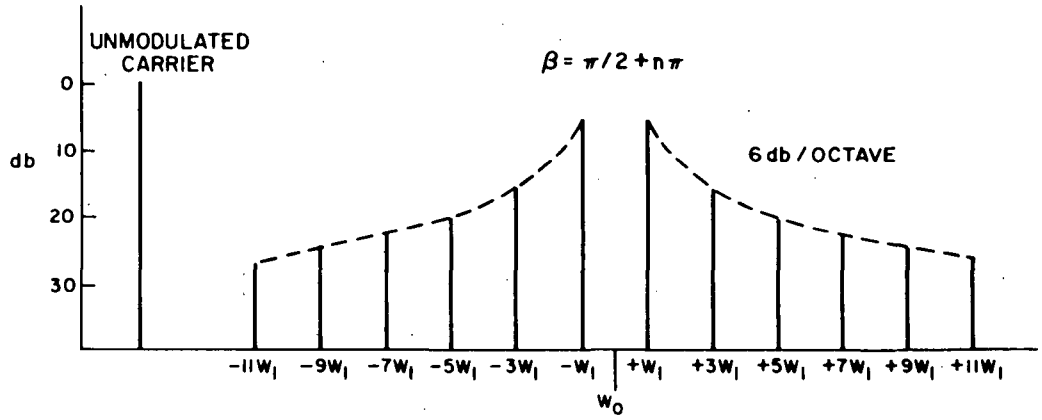

b) TYPICAL SPECTRA FOR SQUARE-WAVE PSK
AS PRODUCED BY A TRIGONOMETRIC FOURIER EXPANSION

Figure 17. ATS PSK modulation experiment.

For a perfectly symmetrical square wave of peak amplitude A, the current

$$i = \frac{4A}{\pi}\left(\sin \omega_1 t + \frac{\sin 3\,\omega_1 t}{3} + \frac{\sin 5\,\omega_1 t}{5} + \cdots \frac{\sin n\,\omega_1 t}{n}\right) .$$

For the precisely symmetrical square wave, there is no energy in the even harmonics.

The carrier phase modulation produced by the instantaneous contributions of the Fourier-series components of the square wave is

$$\theta_t = \frac{4}{\pi}\left(\theta_1 \sin \omega t + \frac{\theta_3}{3} \sin 3\,\omega t + \frac{\theta_5}{5} \sin 5\,\omega t + \ldots\right) = \theta_{0,1} ,$$

since all tones of identical amplitude produce the same modulation index.

In deriving a Fourier expression for square-wave phase modulation (PM), we consider an unmodulated sine-wave carrier represented in terms of instantaneous phase and frequency as

$$i = I \exp (j\,\theta_t) = I \exp (j\,\omega_0 t) ,$$

where the instantaneous phase θ_t is related to the instantaneous frequency ω_t by

$$\theta_t = \int_0^t \omega_t \, dt .$$

For single-tone sine-wave PM, the instantaneous phase

$$\theta_t = \omega_0 t + \Delta\theta \sin \omega_1 t ,$$

so that

$$i_{pm} = I \exp (j\,\omega_o t_1) \exp (j\,\Delta\theta \sin \omega_1 t) .$$

For complex wave modulation, the phase function $\Delta\theta_t$ is introduced into the sinusoidal expression above. This phase modulation function

$$M_p(\Delta\theta_t) = \exp (j\, \Delta\theta \sin \omega_1 t)$$

is introduced so that

$$i_{pm} = M_p(\Delta\theta_t)\, I \exp (j\omega_0 t) \quad .$$

A Fourier series expansion gives

$$i_{pm} = I \sum_{n=-\infty}^{\infty} C_n \exp [j(\omega_0 t + n\omega_1 t)] \quad ,$$

where

$$C_n = \frac{\omega_1}{2\pi} \int_0^{2\pi/\omega_1} \exp (j\theta_t) \exp (-j\, n\omega_1 t)\, dt \quad .$$

Integrating over a square-wave interval

$$0 < t < \pi/\omega_1 \quad , \quad \theta_t = \beta$$

and

$$\pi/\omega_1 < t < 2\pi/\omega_1 \quad , \quad \theta_t = -\beta$$

gives

$$i_{pm} = I \cos\beta \exp (j\omega_0 t) + \frac{2I}{\pi} \sin\beta \sum_{n=1,3,5}^{\infty} \left(\frac{1}{n}\right)$$

$$\exp [j(\omega_0 t + n\omega_1)t] \cdot \exp [(j\omega_0 - n\omega_1)t] \quad .$$

The above expression can be interpreted as a carrier component

$$i_0 = I \cos \beta \quad ,$$

and sidebands of magnitude

$$i_n = \frac{2\, I \sin \beta}{n\pi} \quad , \qquad n = 1, 3, 5, \ldots \quad .$$

For the case under consideration, 0, 1 modulation is used and $2\theta = 180°$. In PM terms,

$$\beta = \Delta\theta = \pi/2 \quad .$$

Under these conditions, the carrier is suppressed, $i_0 = 0$, and the sidebands are odd harmonics diminishing at 6 db/octave. Figure 17b shows the line spectra for this case.

The data recordings of transmissions at each of the modulation test frequencies were correlated, the length of correlation being generally around one digital record (200 msec). The correlation function

$$R(\tau) = \lim_{T \to \infty} \frac{1}{T} \int_0^T v_1(t)\, v_2(t + \tau)\, dt \quad ,$$

where $v_1(t)$ and $v_2(t)$ are the recorded functions at each terminal, is shown plotted as a function of τ in Figure 18a, where $\omega_1/2\pi = 83.3$ kHz.

This correlation function contains only spectral harmonics that are present in both signals $v_1(t)$ and $v_2(t)$. This can be shown easily by considering the generalized signals

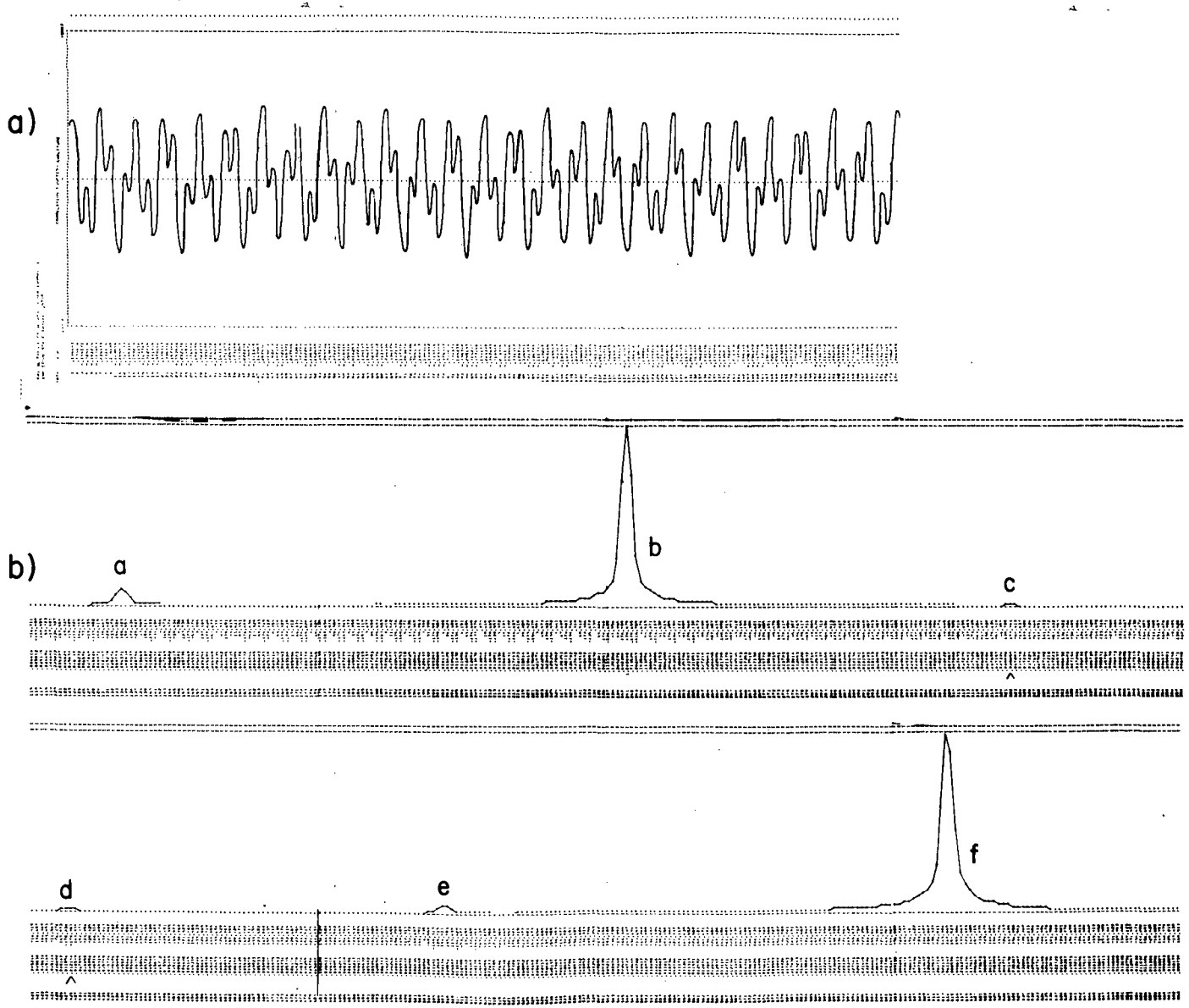

Figure 18. Correlation function (a) and spectrum (b) for 83.3 kHz modulation for ATS 5.

$$v_1(t) = A \cos(\omega_1 t + \theta_1) \quad ,$$

$$v_2(t) = B \cos(\omega_2 t + \theta_2) \quad ,$$

$$v_2(t + \tau) = B \cos(\omega_2 t + \theta_2 + \omega_2 \tau) \quad .$$

Substituting these expressions in the expression above for the correlation function gives

$$R(\tau) = \lim_{T \to \infty} \frac{AB}{2T} \int_0^T \{\cos[(\omega_1 + \omega_2)t + (\theta_1 + \theta_2) + \omega_2 \tau]$$

$$+ \cos[(\omega_2 - \omega_1)t + (\theta_2 - \theta_1) + \omega_2 \tau]\} \, dt \quad .$$

$$R(\tau) = \lim_{T \to \infty} \frac{AB}{2T} \left\{ \frac{\sin[(\omega_1 + \omega_2)T + (\theta_1 + \theta_2) + \omega_2 \tau] - \sin(\omega_2 \tau + \theta_1 + \theta_2)}{\omega_1 + \omega_2} \right.$$

$$\left. + \frac{\sin[(\omega_2 - \omega_1)T + (\theta_2 - \theta_1) + \omega_2 \tau] - \sin[\omega_2 \tau + (\theta_2 - \theta_1)]}{\omega_2 - \omega_1} \right\} \quad .$$

The first term in brackets above is zero in the limit for all realizable (nonnegative) frequencies. The second term is also zero except for the condition

$$\omega_2 = \omega_1 = \omega \quad .$$

The expression for $R(\tau)$ then becomes

$$R(\tau) = \frac{AB}{2} \cos(\omega \tau + \theta_2 - \theta_1) \quad , \quad (\omega_1 = \omega_2)$$

and

$$R(\tau) = 0 \quad , \quad (\omega_1 \neq \omega_2) \quad .$$

Hence, the correlation function plotted contains no cross-frequency terms and is itself composed of the harmonics of the transmitted signal. Identification of the components is difficult from an amplitude plot such as Figure 18a, especially since the phase modulation is not easily seen.

The spectral components can be best identified by a Fourier spectral analysis as shown in Figure 18b. The most prominent features of the spectrum display are lettered. At the precise center of the spectrum, feature d is the vestigial component of the carrier, the RF system having been tuned to present the carrier (1550.00 MHz) at the center of the VLBI system bandpass. The first harmonic sidebands are labeled b and f and are displaced 83.3 kHz on each side of the carrier. The broadening of the spectrum functions is principally caused by incidental amplitude modulation (AM) introduced by the balanced modulator. This simultaneous AM and PM is generally unavoidable in practical systems and produces both an increase in sideband amplitudes and the broadening effect. The third and fifth upper harmonics of the PSK spectrum are outside the passband of the video converter; the third and fifth lower sidebands, however, appear as vestigial components, labeled a and e, respectively. Although they are below the lower cutoff point of the video converter filter, they appear because they are not completely rejected in the 3-MHz image filter. Consequently, they are reflected into the video bandpass, but with their amplitudes reduced about 12 db more than from the expected 6-db/octave rule for harmonics within the video passband. The lower seventh harmonic, being even more attenuated by the image filter, cannot be seen on the plot. The very weak spectral feature at c (143 kHz) is probably the image of the L-band wide-band data-mode frequency, which originates from a spacecraft voltage-control oscillator (VCO) at a nominal 1550.480 MHz and decreases to about 1550.240 MHz in frequency over its period of operation. The received image is at 1550.333 MHz.

Similar correlation functions and spectra are obtained for the cases of square-wave PSK modulation at 8.33 kHz and 833 Hz. The effects of the modulation products of the 833-Hz signal are clearly shown in Figure 19a. The concentration of the products about the center of the video band (190 kHz) results in a basic correlation function of sinusoidal form and monochromatic appearance. The difference frequency between the two first-harmonic sidebands is apparent as a low-frequency envelope over the correlation function at 2×833 Hz or 1.66 kHz. A higher frequency envelope at 47 kHz is a result of an incidental amplitude modulation caused by the balanced modulator. This amount of AM (about 10%) appears constant over all modulation modes.

The spectrum in Figure 19b clearly resolves the two first harmonics, and the much reduced subordinate peaks represent the odd harmonics, which are easily distinguishable and in proper ratio out to the ninth harmonic. Again, the effect of the incidental AM is to broaden the spectral peaks.

The output of the L-band wide-band frequency-translation mode when no PSK modulation is applied is presented in Figure 20. Figure 20a shows about 10% incidental AM of the carrier, which is placed at the video-band center of 190 kHz. Figure 20b is the AM-broadened spectrum of the carrier. To the left of the carrier is seen the image of the L-band wide-band data VCO, which is apparently unmodulated. It is rejected by the image filter to about 30 db below the WBFT carrier in the passband.

As described above, the periods of regular modulation were broken by several short periods of random-noise input to the modulator. Because the L-band uplink transmissions on this experiment were not controlled by SAO, only a few periods of noise transmission were available. However, the broadband nature of this noise made it possible to perform unambiguous correlation analyses over the full 350-kHz bandwidth of the VLBI terminal. The spectral form of the noise was plotted by taking the Fourier transform of the autocorrelation function of the received time series, as illustrated in Figure 21. The result is a bandpass-shaped plot (Figure 22) closely matching the bandpass characteristics of the video converter, which is shown in

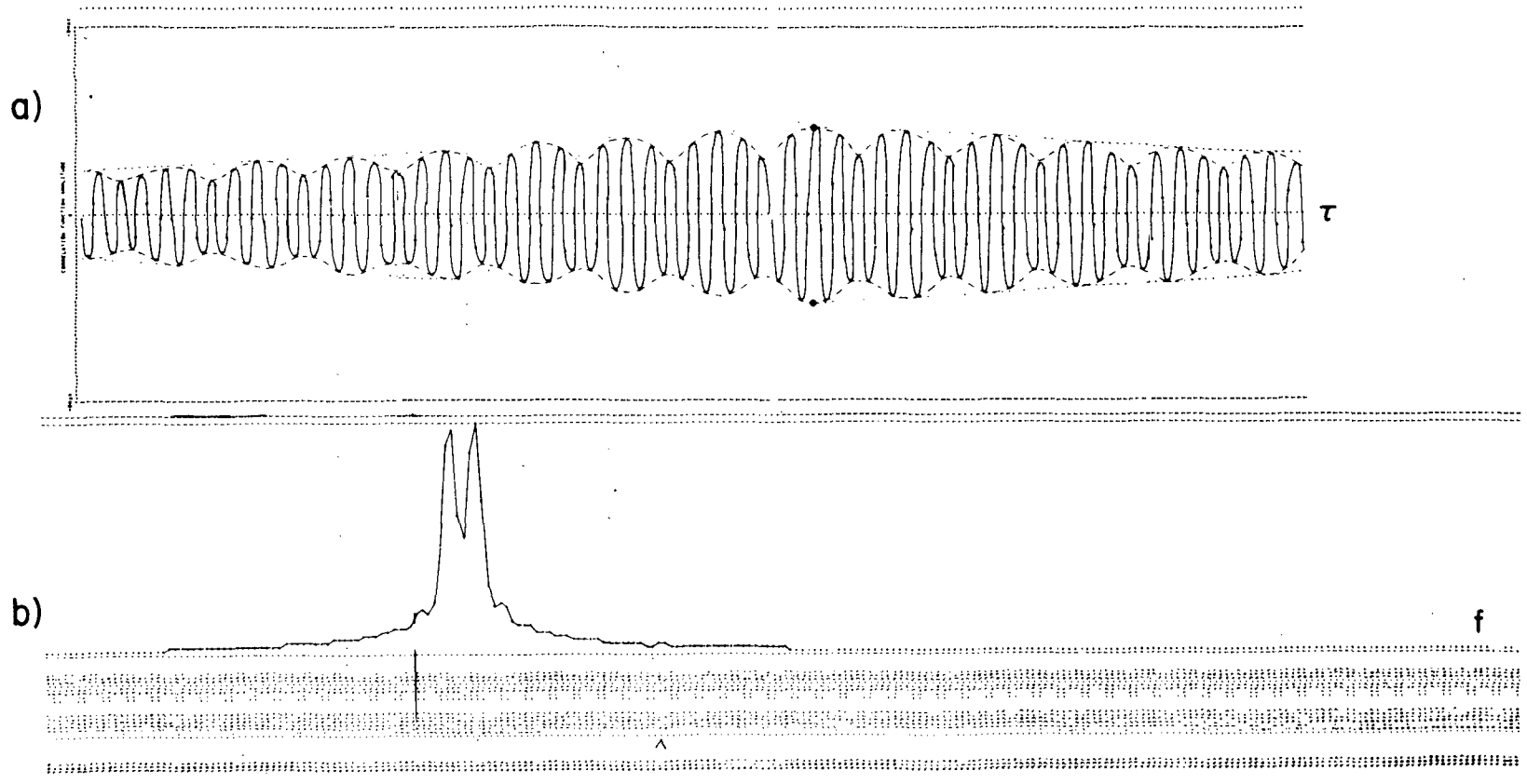

Figure 19. Correlation function (a) and spectrum (b) for 833 Hz PSK modulation.

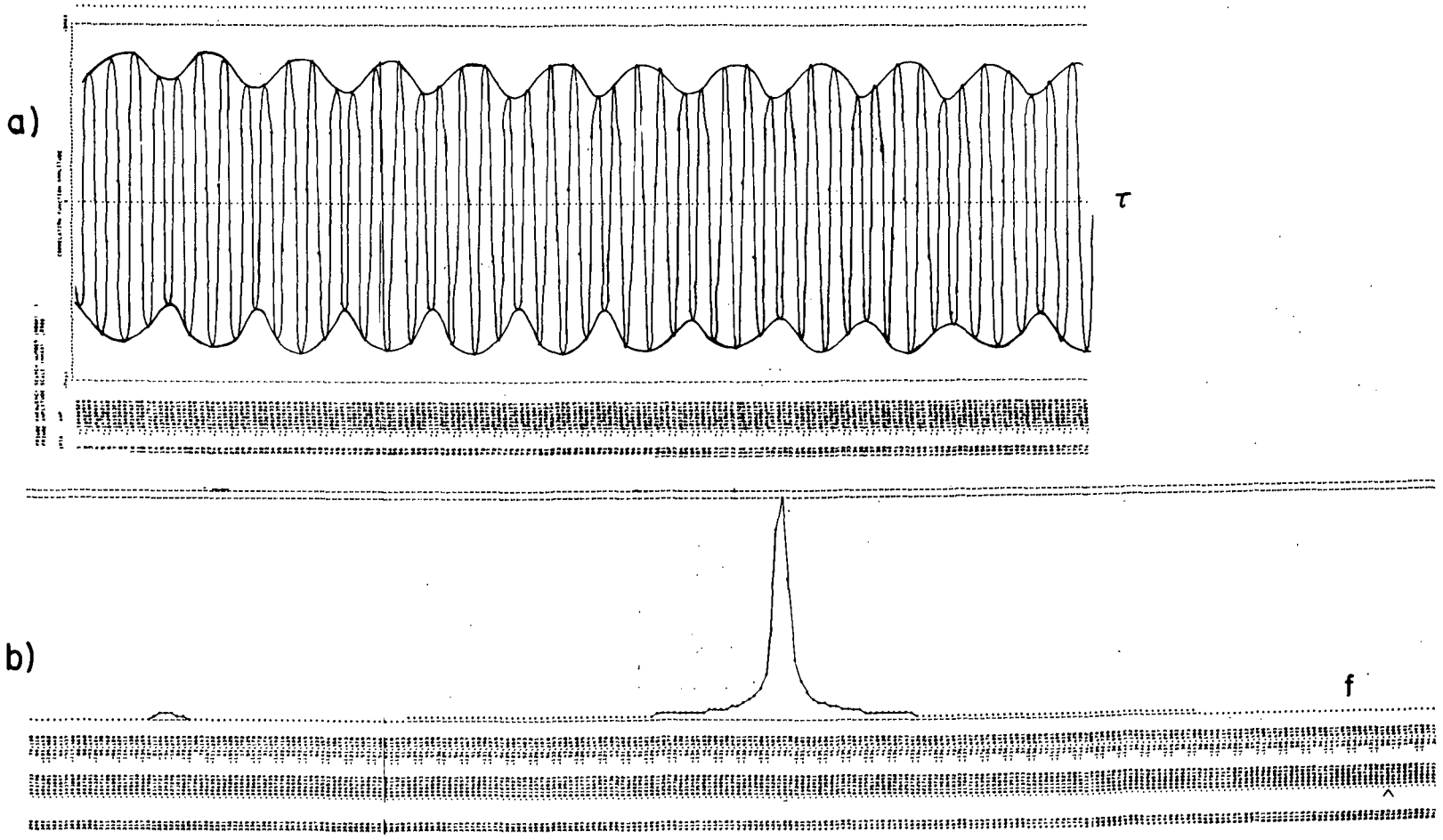

Figure 20. Correlation function (a) and spectrum (b) for zero modulation ATS 5.

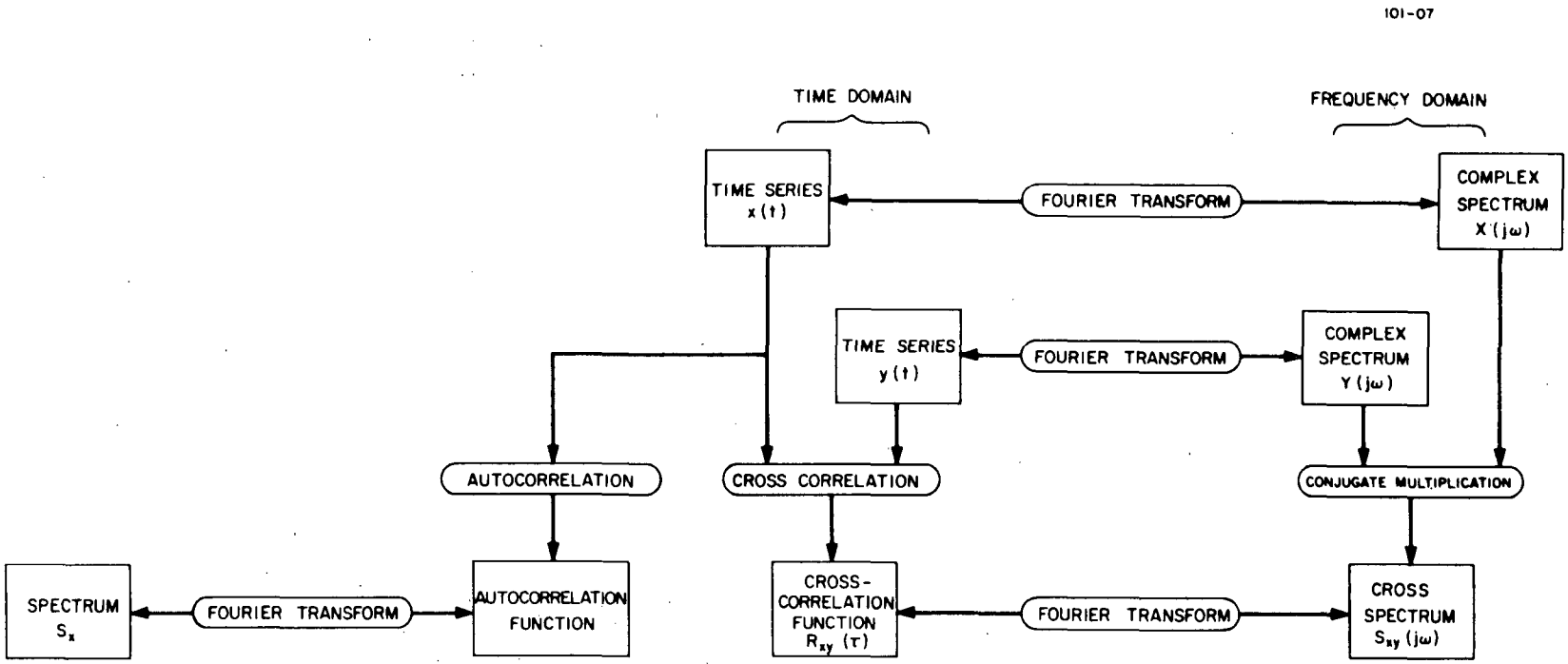

Figure 21. Time and frequency-domain relationships used in data analysis.

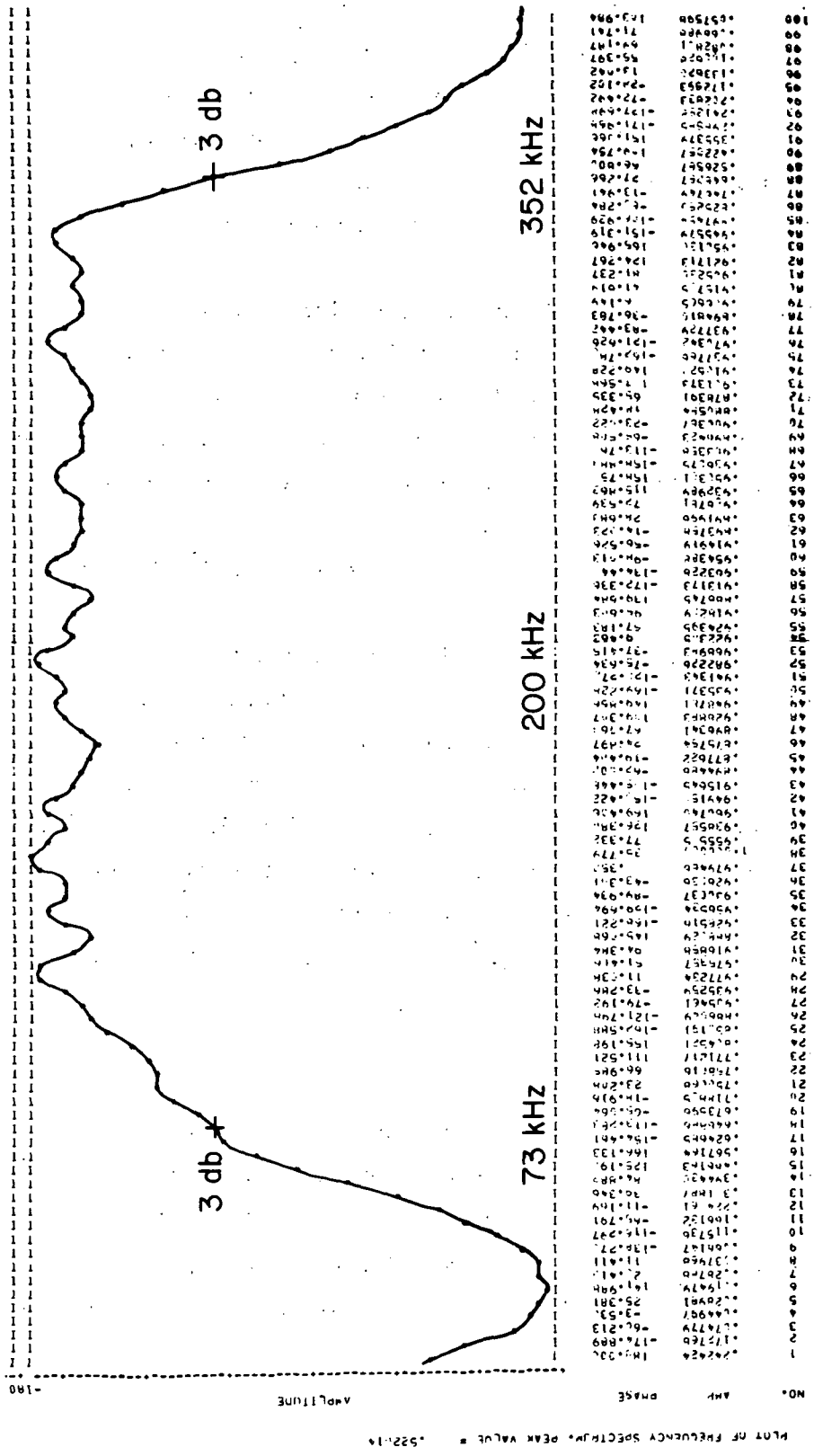

Figure 22. ATS 5 noise spectrum.

Figure 23. It is approximately 280 kHz wide at the 3-db points, with about ±0.5-db ripple in the passband. The irregularities are mainly caused by the fact that only a single digital record was used to compute the spectrum of Figure 22. However, the response at DC (zero frequency) appears to indicate that the clipper sampler has a small DC bias. Attempts to detect correlatable periods of voice or data transmission were unsuccessful.

Correlation plots produced from selected individual records (~150,000 bits) of the noise modulation are shown in Figure 24. The record numbers refer to the digital records depicted in Figure 16, which correspond to different portions of the antenna sweep period. Naturally, the correlation function is a maximum when the digital record on which it is based occurs at the peak of the signal, and a minimum when only a small portion of the record contains a signal. No correlation was discernible for records 358, 359, 362, and 363.

These correlation plots represent the amplitude of the correlation without reference to phase. Since all records were included in a span of 2 sec of observation time, the incremental time delay τ_d of the functions is constant to within the resolution of the measurement and equals 32.2 μsec. Most of this time shift is accounted for by the known synchronization of the station clocks, which amounted to 35 μsec at the epoch of observations. The residual delay δ_T, then, is 2.8 μsec. Additional observations over a second baseline and range information would be required to calculate satellite position.

5.2.4 Technical summary

The computer analysis of the modulation-signal properties has demonstrated that the RF, IF, and video-band phase and amplitude properties of the system are acceptable. It has also shown that the performance of the timing, sampling, and recording components is satisfactory. This was done on a transcontinental baseline with totally independent processing and timing equipment.

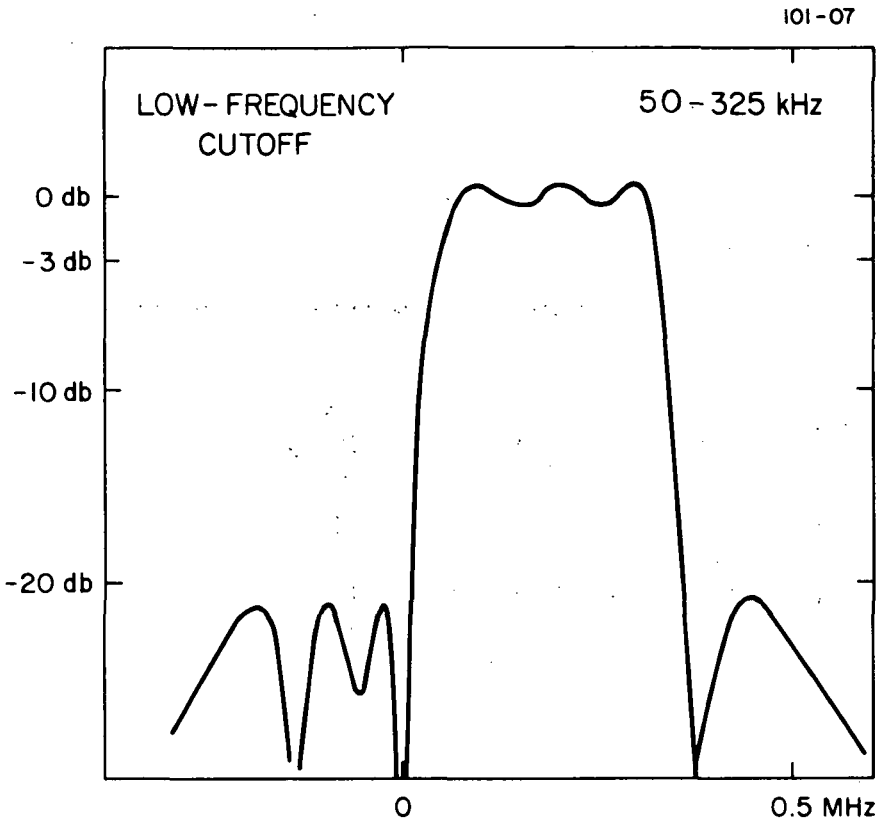

Figure 23. Bandpass characteristics of video-converter low-frequency channel.

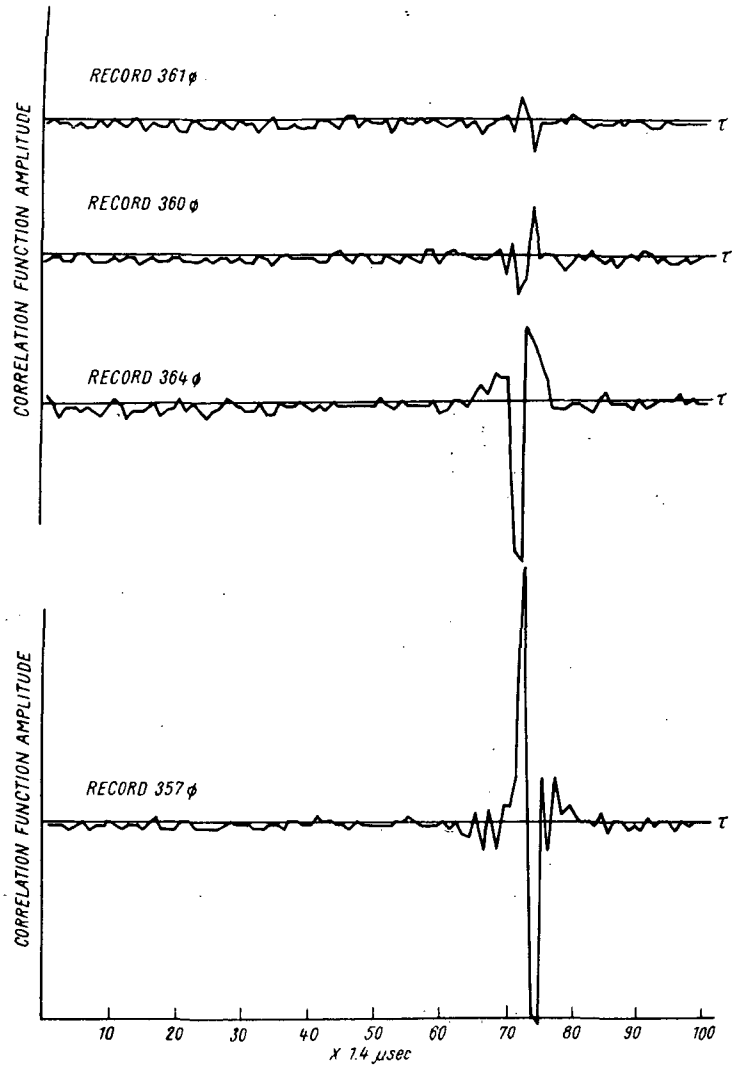

Figure 24. Correlation functions for noise modulation for ATS 5.

In addition, time-delay interferometric measurements were made that were indicative of system performance sufficient to define satellite positions to within 20 m with the addition of a third station to the baseline network.

5.3 Later Long-Baseline Results

In cooperation with NASA/GSFC, three subsequent observing sessions were successfully completed under Contract NAS 5-20247. These sessions are listed below with the type of source and the receiver band used.

Session	Date	Source	Receiver frequency	Baseline
I	6 May to 5 June 1971	ATS 1, ATS 3, and natural sources	C-band	Rosman, North Carolina Mojave, California
II	19 August to 1 September 1971	natural sources	C-band	Rosman, North Carolina Agassiz, Massachusetts Mojave, California
III	28 February to 8 March 1972	ATS 1, ATS 3, and natural sources	C-band	Agassiz, Massachusetts Owens Valley, California

These results are briefly mentioned to indicate the success of the instrumentation and techniques developed under Contract NSR 09-015-079. From Session I and Session III, the geocentric coordinates of the ATS satellites have been found to an accuracy of ±70 m and their orbital parameters resolved with an accuracy equivalent to or better than that possible with range and range-rate tracking [12, 13]. The natural and artificial (satellite) radio sources observed in Sessions II and III have been used to construct three-dimensional baselines between transcontinental stations with a consistency of ±22 m at C-band frequencies, by using both time-delay and fringe-rate processing of narrow-bandwidth data.

6. REFERENCES

[1] Smithsonian Astrophysical Observatory, Investigation of Continental Drift, Phase I Effort Final Report, Contractor Report, Contract NSR 09-015-079, November 1968.

[2] Smithsonian Astrophysical Observatory, Investigation of Continental Drift, Phase II Effort Final Report, Contractor Report, Contract NSR 09-015-079, April 1969.

[3] Smithsonian Astrophysical Observatory, The Application of VLB Interferometry to Earth Measurements, Phase III Effort Final Report, Contractor Report, Contract NSR 09-015-079, December 1969.

[4] Smithsonian Astrophysical Observatory, The Application of VLB Interferometry to Earth Measurements, Progress Report No. 1, Contractor Report, Contract NSR 09-015-079, May 1970.

[5] Weinreb, S., A Digital Spectral Analysis Technique and Its Application to Radio Astronomy, Massachusetts Institute of Technology, Cambridge, Mass., RLE Tech. Rep. 412, 119 pp., August 1963.

[6] Bare, C. C., VLB Control II, National Radio Astronomy Observatory, Green Bank, W. Va., Electronics Division Internal Rep. No. 66, December 1967.

[7] Bare, C. C., VLB Delay II, III, National Radio Astronomy Observatory, Green Bank, W. Va., Electronics Division Internal Rep. No. 67, January 1968.

[8] Michelini, R. D., A One-Bit VLBI Recording and Playback System Using Videotape Recorders, Radio Sci., vol. 5, p. 1263, 1970.

[9] Moran, J. M., Interferometric Observations of Galactic OH Emission, Massachusetts Institute of Technology, Electrical Engineering Dept., Ph.D. Thesis, 1968.

[10] Levine, M. W., and Vessot, R. F. C., Hydrogen-Maser Time and Frequency Standard at Agassiz Observatory, Radio Sci., vol. 5, p. 1287, 1970.

[11] Rogers, A. E. E., Very Long Baseline Interferometry with Large Effective Bandwidth for Phase-Delay Measurements, Radio Sci., vol. 5, p. 1239, 1970.

[12] Ramasastry, J., Rosenbaum, B., Michelini, R. D., Frost, D., Ross, S., and Boornazian, A., Tracking of the ATS-3 Synchronous Satellite by the Very Long Baseline Interferometer (VLBI) Technique, Goddard Space Flight Center X-553-72-290, July 1972.

[13] Rosenbaum, S., The VLBI Time Delay Function for Synchronous Orbits, Goddard Space Flight Center X-553-72-286, July 1972.